Published in final edited form as:
Mass Spectrom Rev. 2010 ; 29(3): 503–521. doi:10.1002/mas.20272.

The Role of Mass Spectrometry-Based Metabolomics in Medical Countermeasures Against Radiation

Andrew D. Patterson[a], **Christian Lanz**[b], **Frank J. Gonzalez**[a], and **Jeffrey R. Idle**[b,*]

[a]Laboratory of Metabolism, Center for Cancer Research, National Cancer Institute, Bethesda, MD
[b]Institute of Clinical Pharmacology and Visceral Research, University of Bern, 3010 Bern, Switzerland

Abstract

Radiation metabolomics can be defined as the global profiling of biological fluids to uncover latent, endogenous small molecules whose concentrations change in a dose-response manner following exposure to ionizing radiation. In response to the potential threat of nuclear or radiological terrorism, the Center for High-Throughput Minimally Invasive Radiation Biodosimetry (CMCR) was established to develop field-deployable biodosimeters based, in principle, on rapid analysis by mass spectrometry of readily and easily obtainable biofluids. In this review, we briefly summarize radiation biology and key events related to actual and potential nuclear disasters, discuss the important contributions the field of mass spectrometry has made to the field of radiation metabolomics, and summarize current discovery efforts to use mass spectrometry-based metabolomics to identify dose-responsive urinary constituents, and ultimately to build and deploy a noninvasive high-throughput biodosimeter.

Keywords

Biodosimetry; ionizing radiation; metabolomics

I. INTRODUCTION

Accidental or intentional exposure to ionizing radiation is a major, worldwide public health concern that requires substantial efforts on many fronts (e.g., local, state, and federal law enforcement, emergency preparedness, policy makers, and basic and translational medicine and science) to prevent unwanted exposures as well as to develop contingencies to manage and treat exposed individuals (Commission on the Prevention of Weapons of Mass Destruction Proliferation and Terrorism (U.S.), 2008, Conklin & Liotta, 2005, Dorr & Meineke, 2006). Additionally, the very real and increasing threat of a terrorist attack with a nuclear or radiological weapon urges the development and implementation of strategies for mass screening of exposed individuals in order to determine rapidly and accurately the absorbed radiation dose (Blakely et al., 2005, Conklin & Liotta, 2005, Pellmar & Rockwell, 2005). Moreover, it will be critical and challenging to differentiate individuals exposed to potentially harmful doses from those who suffer only from psychological effects and other traumas. To this end, the Center for High-Throughput Minimally-Invasive Radiation Biodosimetry (CMCR) (http://cmcr.columbia.edu/), funded by the Department of Health and Human Services, Office of Public Health Emergency Medical Countermeasures, and the

*Address for correspondence: Institute of Clinical Pharmacology and Visceral Research, University of Bern, Murtenstrasse 35, 3010 Bern, Switzerland; jidle@ikp.unibe.ch; Tel: +420 603 484 583; Fax: +420 220 912 140.

National Institutes of Health and coordinated by the National Institute of Allergy and Infectious Diseases (http://www3.niaid.nih.gov/topics/radnuc), was established at Columbia University, New York to develop new high-throughput radiation biodosimetry assays and tools that are field-deployable for mass population screening scenarios. Beyond nuclear terrorism, the development of noninvasive radiation biomarkers will be of value to study environmental exposures and to the field of radiation oncology, as well as for extensive manned space exploration (e.g., manned missions to Mars) (Straume et al., 2008).

Whereas accidental and intentional exposures are both relatively rare, there are well-documented examples that provide clear and compelling reasons for the development of radiation exposure biomarkers as well as for the design, development, stockpiling, and deployment of portable measuring devices to rapidly screen populations in the event of a radiological disaster. The events outlined below represent a fraction of the total number of nuclear accidents to date, and are mentioned here to demonstrate different scenarios of radiation exposure on a range of scales in terms of radiation quantities and the number of people exposed and/or affected.

II. HUMAN EXPOSURES TO RADIATION – ACTUAL AND THEORETICAL

A. Nuclear Weapons and the Potential of Widespread Exposures

The detonation of the “Little Boy” atomic bomb (equivalent to 13 kt of TNT) over Hiroshima on August 6, 1945 is estimated to have killed 140,000 people, and that of the “Fat Man” bomb over Nagasaki three days later very likely killed a further 80,000 inhabitants. In addition, deaths from 231 leukemias and 334 solid malignancies have been attributed to radiation fallout from these nuclear events (Schull, 1998). The precise morbidity and mortality attributable to the use of these atomic weapons might never be fully realized.

Nearing the end of the Cold War, the USSR built and deployed six 941 Akula submarines, each with the capability to carry 20 submarine-launched ballistic missiles (SLBMs), each with up to 10 nuclear warheads that had individually the explosive power of fifteen Hiroshima bombs. This submarine fleet had the capability to wreak nuclear devastation on the scale of 18,000 Hiroshima bombs. In contrast, the US deployed a total of 408 Trident I and II SLBMs with a total explosive yield equivalent to over 50,000 Hiroshima bombs. The airborne and land-based nuclear bombs and missiles considerably multiply this total nuclear yield of the two major superpowers. The US nuclear stockpile alone has been estimated to have the capacity of 1.5 million Hiroshima bombs (Zoellner, 2009). Several other countries, notably the UK and France, also possess significant nuclear arsenals. Utilization of nuclear weapons on this scale would yield an Armageddon that would not require medical countermeasures. However, a single nuclear device deployed by a terrorist group or agents of a failed state would produce a large number of casualties in the immediate blast area, but would also expose peripheral individuals to the effects of ionizing radiation and nuclear fallout. It is in such a scenario that first responders would benefit from high-throughput noninvasive radiation biodosimetry devices to fractionate this population into those who would benefit from therapeutic intervention or palliative care and those whose radiation dose had been too trivial to mandate emergency treatment.

The most powerful single nuclear weapon ever tested was the “Tsar Bomba”, a 50 Mt hydrogen bomb (~4,000 Hiroshima bombs) that was detonated by the USSR in the Novaya Zemlya archipelago on October 30, 1961 (Sakharov, 1990). This bomb was a highly efficient device (97%), and so there was relatively little nuclear fallout of unspent isotopes. It should be noted that the size of this bomb was equivalent to ten-times all the explosives used in World War II. In contrast, “Castle Bravo” was the most powerful nuclear device ever detonated by the USA (15 Mt; ~1,200 Hiroshima bombs) at Bikini Atoll, Marshall

Islands on March 1, 1954. This unexpectedly high yield, due to a miscalculation on the part of its designers, led to the largest "accidental" environmental radiological contamination due to the United States, with the nuclear fallout over 18,000 square kilometers (about the size of New Jersey) that affected local islanders and visiting Japanese fishermen, many of which grew ill and one eventually died (Keever, 2004, Titus, 2001).

In addition to nuclear bombs, there exist devices known colloquially as "dirty bombs", which are simply radiological dispersal devices that combine radiological material and conventional explosive. Much easier to obtain and assemble, dirty bombs are likely candidates for terrorist use. The main immediate casualties of a dirty bomb are due to the explosion itself; the range of dispersed nuclear material will depend on prevailing factors, such as site of detonation and weather conditions, including wind direction. The spread of radioactive materials might be expected to be no more than a few city blocks or, at most, a few miles, in contrast to a nuclear explosion which might affect hundreds or even thousands of square kilometers.

B. Nuclear Accidents and the Potential of Local Exposures

Perhaps the best-known and most catastrophic example of a nuclear reactor disaster in history is the Chernobyl Nuclear Power Plant (near Prypiat, Ukraine) on April 26, 1986, when reactor #4 exploded (International Atomic Energy Agency, 2008). Nearly 200,000 square kilometers of the USSR, especially in Belarus, Ukraine, and Russia, were contaminated with radioactive ^{131}I (8-day half-life) and ^{137}Cs (30-year half-life) that affected hundreds of thousands of people, including Chernobyl employees, liquidators (recovery workers), and residents in and around the exclusion zone as well as in neighboring countries. Whole-body dose estimates vary considerably, and range from negligible amounts above background levels to upwards of 20 Gray (Gy) (especially with the first responders). Estimates, in terms of the ultimate death toll, vary a great deal and are controversial; however, anywhere between 4,000 and 10,000 deaths might ultimately be attributed to the Chernobyl disaster (Mousseau et al., 2005, Stephan, 2005). Perhaps the best lesson learned here was that there were no established guidelines or procedures for emergency personnel when they handle radiological disasters on such a large scale, including biological assays and physical dosimetry (Chumak, 2007). Other examples include the accident at the Tokai-mura uranium-processing facility (Ibaraki Prefecture, Japan) and the partial meltdown at the Three Mile Island Nuclear Generating Facility (Dauphin County, Pennsylvania). Although these events are relatively small compared with Chernobyl, they still represent the worst nuclear events for Japan and the United States.

The radioactive source from an abandoned radiotherapy machine used in the Instituto Goiano de Radioterapia in Goiânia, Brazil was dismantled by scrap-metal scavengers, and 93 g of highly radioactive [^{137}Cs]cesium chloride granules was removed and handled by adults and children (International Atomic Energy Agency, 1988). In all, 249 people were exposed, 4 died, and approximately 112,000 people had to be screened for radiation exposure. Doses ranged from 0 to 7 Gy, and this incident marked the first time a medical countermeasure (Prussian Blue, Radiogardase®) was used (Melo et al., 1994). Radiogardase® is the first FDA-approved medical countermeasure against ^{137}Cs and ^{201}Tl contamination to be used in case of, say, exposure to a dirty bomb to reduce the residence time of these isotopes in the body by a factor of 2–3 (Faustino et al., 2008, Yang et al., 2008). The Goiânia incident clearly points to the accidental exposure risks associated with the many unsecured, missing, or stolen radiological devices across the world.

In Moscow, Russia, Chechen rebels threatened to explode in Izmailovsky Park a dirty bomb that contained ^{137}Cs. Fortunately, the bomb was dismantled and the ^{137}Cs was secured without incident. Although radiological dispersal devices (e.g., dirty bombs) are probably

most effective as psychological weapons as opposed to causing harm from exposure to radiation, they do present a problem for emergency preparedness and first-responders. That is, how does one quickly and accurately identify those individuals who have received a substantial dose requiring treatment and follow-up from those who present with psychosomatic symptoms?

These unfortunate events have been invaluable in broadening our understanding of radiation and its biological effects on Man. With the impending threat of nuclear terrorism, these events serve as ominous warnings that urge the establishment of better, more efficient emergency preparedness scenarios for radiological disasters, and the development of rapid, accurate, and high-throughput biodosimetry.

III. CURRENT METHODS OF RADIATION BIODOSIMETRY

Much of what is known about the effects of ionizing radiation on humans comes from studies of survivors from the events described above, from survivors of Hiroshima and Nagasaki, and from patients undergoing radiotherapy (Hall & Giaccia, 2006). Data collected from those individuals have been useful to establish the $LD_{50/60}$ (the dose at which 50% will survive 60 days after exposure) and the overt symptoms of acute radiation syndrome (ARS). Following exposure to ionizing radiation, the symptoms immediately following (minutes), and up to days or weeks after, are useful to understand the radiation-exposure event, including total absorbed dose (Blakely, et al., 2005, Hall & Giaccia, 2006). Phases of ARS might include, particularly at higher doses, prodromal symptoms such as nausea, vomiting, and their time-of-onset (often referred to as time-to-emesis), and these symptoms are useful to establish the whole-body dose and the subsequent triage of victims. The Armed Forces Radiobiology Research Institute (AFRRI) developed the Biodosimetry Assessment Tool (BAT) and a field-deployable version, the First-Responder Radiological Assessment Triage (FRAT), to record symptoms after a radiation-exposure incident (Goans & Waselenko, 2005, Sine et al., 2001). Other useful measurements include lymphocyte-depletion kinetics, as well as other symptoms associated with hematopoietic syndrome (2.5–5 Gy), gastrointestinal syndrome (5–12 Gy), and cerebrovascular syndrome (>100 Gy). What is important to point out here is that not one measurement is adequate for dose determination; rather, a collection of measurements, including physical and biological dosimetry, and the use of field-deployable devices, will be of great use for first-responders to triage victims onsite.

The method of choice, and still the “gold standard” to determine absorbed dose, is the dicentric assay that is based on chromosomal aberrations of cultured peripheral blood lymphocytes (PBLs) following exposure to ionizing radiation. In fact, AFRRI and the World Health Organization (WHO) have developed standardized protocols and reference laboratories to perform the assay on a large scale should a radiological disaster occur (Blakely et al., 2009). This assay, although useful, remains a less than ideal tool for immediate triage of overexposed individuals. It is not field-deployable, because it requires PBL culture, and the preparation and scoring of the metaphase spreads; even with automation, it requires nearly 3 days to complete (Paul & Amundson, 2008). However, the dicentric assay is an indispensable tool and should remain as part of the biodosimetry suite of assays, albeit downstream in the biodosimetry pipeline.

Many alternatives to the dicentric assay are currently under investigation and are in the early stages of product development (also as part of the Columbia CMCR project). One of the best and most promising examples is the development of gene expression signatures from isolated PBLs, and the development of lab-on-a-chip platforms (Amundson et al., 2001, Amundson et al., 2001, Amundson et al., 1999, Amundson et al., 2000, Amundson &

Fornace, 2001, Amundson & Fornace, 2003, Liu et al., 2004). Stress gene signatures have been useful for dose assessment, and most importantly, without the need to establish a gene expression baseline signature. An example of the lab-on-a-chip biodosimeter for gene expression studies can be found here - http://cmcr.columbia.edu/project2.html.

Whereas these approaches have intrinsic value (and an extensive history) in radiation biodosimetry, the novel application of a mass spectrometry-based analysis of easily obtainable biofluids such as urine, sweat, and/or sebum might provide a simple, noninvasive biodosimeter. In the coming sections, radiation metabolomics will be discussed in terms of what is currently known, new bioinformatic approaches that have evolved from a study of the radiation metabolome, and where progress currently stands in the identification of a robust and reliable metabolomic signature that is associated with ionizing-radiation exposure. Particular emphasis will be placed on the radiation biomarker discovery phase using metabolomics.

IV. RADIATION METABOLOMICS

A. What is Metabolomics?

Metabolomics is a rapidly evolving field that aims to identify and quantitate changes in small-molecule concentrations (arbitrarily <850 Da) that are known collectively as the metabolome. Just as gene expression differs across the various cell types of the body, the metabolome is also context-dependent; that is, it varies from individual to individual, organ to organ, cell type to cell type, and, importantly, in response to disease processes and external provocations. Furthermore, and perhaps one of the greatest challenges to the field of metabolomics will be understanding the influence of age, gender, diet, and genetic polymorphisms on the various human metabolomes (e.g., urine, sebum, serum, plasma, sweat) (Lawton et al., 2008). No single analytical platform can capture the whole metabolomic complement of a tissue or body fluid. Various NMR methodologies have been applied to metabolomic profiling, including ^{1}H, ^{13}C, ^{15}N, and ^{31}P NMR. Most importantly, LC-MS, GC-MS, and CE-MS platforms have all been employed, and it must be stated that metabolomics in practice is merely the combination of high-end analytical chemistry with the mathematical and statistical evaluation of the resultant-data matrices. In theory, an HPLC assay that visualized only 20 peaks in plasma samples could be used as the front-end of a metabolomic investigation, although one suspects that visual inspection of the chromatograms is equally likely to reveal enriched or depleted analytes.

Although the metabolome represents an untapped resource for biomarker discovery as well as to determine therapeutic endpoints, our current knowledge of the metabolome and its altered flux is limited. Moreover, metabolome characterization is an essential addition to the other “omics” disciplines such as genomics, transcriptomics, and proteomics to generate and represent a true systems-biology perspective of organismal and cellular physiology and disease (Ellis et al., 2007). The anticipated contribution of metabolomics to the field of science and ultimately to health care is highlighted by its prominence in a recent NIH Roadmap (Zerhouni, 2003).

B. Metabolomic Platforms

The application of mass spectrometry to metabolomics has been expertly reviewed (Dettmer et al., 2007). Below are highlighted some of the salient features and contributions of the platforms that are commonly deployed in metabolomics investigations.

1. NMR—Nuclear magnetic resonance (NMR) is one of the most powerful analytical techniques in the biological sciences. Its potential sophistication is evidenced by the fact that

3D- and 4D-NMR experiments have led to the solution structures of over 100 plant proteins (Eisenreich & Bacher, 2007). The contribution of ^{1}H nuclear magnetic resonance (NMR) to the field of metabolomics cannot be overlooked, and it would be inappropriate to not mention some of the advances that can be attributed to ^{1}H NMR-based metabolomics (Coen et al., 2008, Nicholson & Lindon, 2008). Some of the initial observations from radiation exposure that can be assessed by changes in the cellular and urinary metabolome were identified with ^{1}H NMR (Yushmanov, 1994). Additionally, the most important advancement or introduction from NMR-based studies was the idea of noninvasive profiling of easily and readily obtainable biofluids such as urine and blood.

NMR is not a separation technology and, therefore, individual signals attributable to each identifiable analyte in a complex mixture must be resolved, often with 2D-NMR experiments and very high field instrumentation, such as 800 MHz or above (Duarte et al., 2009). The purpose of a metabolomic investigation is to obtain as broad a coverage of the small molecules in a sample set as possible. Although NMR lends itself to high throughput with little sample preparation, the abiding weakness of NMR-based metabolomic studies is its focus on the “usual suspects”, a small group of about 30 analytes that occurs with uncanny frequency in most published studies, and includes, for example, citric acid, creatine, creatinine, taurine, 2-oxoglutaric acid, lactic acid, glucose, hippuric acid, succinic acid, trimethylamine *N*-oxide, and certain amino acids (Patterson & Idle, 2009, Robertson, 2005). The tracking by ^{1}H NMR in rodent urine of the concentration changes of certain of these “usual suspects” in relation to a specified provocation has yielded biomarkers, for example, to hepatic and renal toxicity (Holmes et al., 2000, Park et al., 2009, Serkova & Christians, 2005). However, these biomarkers might reveal few mechanisms of the toxic processes under investigation.

Greater coverage of the metabolome, which for urine might comprise 10^{3} to 10^{4} constituents, and for cellular/tissue metabolomes, 10^{5}–10^{6} discrete molecules, requires high-resolution separation technology that can be delivered by ultra-performance liquid chromatography (UPLC) and gas chromatography (GC). Moreover, this classical chromatographic separation of analytes followed by their specific detection, typically with mass spectrometry (MS), has yielded the highly successful analytical platforms of UPLC-MS and GC-MS. That notwithstanding, chromatographic resolution of a complex mixture such as a biofluid into hundreds or thousands of detectable entities, is a technology that is half a century old. The current state-of-the-art chromatographic resolution of analytes tends to be slow; ca. 10 min for UPLC and 30–60 min for GC. Chromatography does not lend itself well to the development of high-throughput strategies for metabolome interrogation in large human populations. The great advantage of MS technologies is that, once ions can be derived from a biological matrix, they can be separated in a matter of seconds on the basis of their *m/z* and accurate mass. Analytical platforms based upon ion resolution rather than chemical resolution are discussed in section IV.B.4 below.

2. UPLC-MS—High-performance liquid chromatography-coupled mass spectrometry (LC-MS) with electrospray ionization (ESI) is a ubiquitous technology. The reduction in particle size of the stationary phase from the standard 5 μm to <2 μm has the consequence of creating increased back pressure (i.e., >40 MPa) but has the advantage of improved chromatographic performance (Xiang et al., 2006). Reduced particle size has necessitated the development of specialized columns and solvent-pumping systems that can withstand pressures up to 100 MPa (~1,000 atmospheres). The Waters ACQUITY system employs 1.7 μm particle size columns, and is referred to as ultra-performance liquid chromatography (UPLC®). Compared to traditional HPLC (i.e., <40 MPa), the run time and solvent usage of UPLC can be reduced fourfold. The UPLC system provides an ideal front end to an MS system for metabolomics analysis. When combined with an orthogonal quadrupole time-of-

flight mass spectrometer (QTOFMS), the resultant UPLC-ESI-QTOFMS provides high chromatographic resolution combined with accurate mass determination (via TOF) to facilitate biomarker identification. In a biofluid such as urine, 3,000–5,000 both positive $[M+H]^+$ and negative $[M-H]^-$ ions might be registered for each sample in a 10-min chromatogram. Some of these ions are in-source fragments, and others are typically Na^+ and NH_4^+ adducts in positive-ion ESI and the occasional dimers. Common negative mode ESI adducts include chloride $[M+Cl]^-$. However, in-source fragments and adducts also provide useful information for final structure determination. Actual molecules in a sample may be far less. Nevertheless, UPLC-ESI-QTOFMS delivers a data-rich output that can be readily mined for biomarkers. The generation of ions by electrospray ionization in both positive (ESI+) and negative (ESI-) modes is a well-tested technology that might be harnessed to discover and ultimately, via targeted metabolite profiling, to detect specific radiation metabolomic signatures in the field. The latter diagnostic stages will likely employ some form of ion resolution device (see below) thus eliminating the need for chromatographic separation.

3. GC-MS—The 1952 Nobel Prize in chemistry was awarded jointly to the British chemist Archer John Porter Martin and the British biochemist Richard Laurence Millington Synge for the development of partition chromatography and its use in the separation of amino acids; that method lead to the earliest amino acid sequence determination of peptides.

At that time, Martin had begun translating his work on liquid-liquid partition chromatography into gas-liquid chromatography (GLC), and succeeded to separate the series of amines in the order of their boiling points; ammonia, monomethylamine, trimethylamine and dimethylamine (James & Martin, 1951); they subsequently used GLC to quantitate these amines (James & Martin, 1952), rapidly applying their method to the separation and quantitation of C_1 to C_{12} fatty acids (James & Martin, 1952). Perhaps the earliest metabolic-profiling published reports were the application of this GLC methodology to determine the component fatty acids on the human forearm (James & Wheatley, 1956) and the skin of laboratory rodents (Wheatley & James, 1957); those data predated metabolomics by half a decade.

The fusion of GLC and MS instruments into GLC-MS in 1964 led to the first published biomedical applications in 1966 from laboratories in Sweden (Eneroth et al., 1966) and the US (Dalgliesh et al., 1966). Dalgliesh and coworkers remarked, “Combined gas chromatography-mass spectrometry gives a diagnostic tool of great power in the evaluation of metabolic patterns….” This landmark paper has been considered to be the birth of metabolomics (http://masspec.scripps.edu/metabo_science/timelines/1966.php).

Modern GC-MS has two different arms that are of value in metabolomics. First, traditional GC-MS with electron-impact ionization (EI) gives a molecular ion ($M^{+\bullet}$) for the vast majority of organic molecules that fragments to produce a mass spectrum that is characteristic of the compound under investigation. Databases such as the NIST/EPA/NIH Mass Spectral Library (220,460 EI spectra from 192,108 compounds) can be accessed to assist in biomarker identification. Second, hybrid GC-TOFMS instruments can yield accurate masses for chemically derivatized analytes that assist in the identification of biomarkers, especially with the assistance of software such as Seven Golden Rules (Kind & Fiehn, 2007) and SetupX (Scholz & Fiehn, 2007). However, it was concluded recently that current databases are unable to retrieve all known metabolites (Kind et al., 2009). Nevertheless, derivatization of metabolome extracts, and separation and analysis on various GC-MS platforms, can yield excellent metabolomic data (see Section D5).

4. Ion-Resolution Technologies—Ion mobility spectrometry (IMS) comprises a set of technologies to separate charged species in the absence of chromatography. There are four IMS methodologies, namely, drift-time ion mobility spectrometry (DTIMS), aspiration ion mobility spectrometry (AIMS), differential-mobility spectrometry (DMS), which is sometimes referred to as field-asymmetric waveform ion mobility spectrometry (FAIMS), and traveling-wave ion mobility spectrometry (TWIMS). IMS separates ions on the basis of their size/charge ratios and of their interaction with a buffer gas (Kanu et al., 2008). IMS has the advantage of speed of analysis and the potential to measure simultaneously significant numbers of positive and negative ions. The deployment of IMS requires a front-end, in which ions are generated from a sample matrix, and an ion-detection system. Commonly, therefore, IMS has been combined with either GC (Kanu & Hill, 2008) or MS (Kanu, et al., 2008). This latter configuration, referred to as IMMS, has been further combined with direct-infusion ESI to produce a so-called ambient-pressure ion mobility spectrometer (APIMS) that was coupled to a time-of-flight mass spectrometer. This APIMS-TOFMS was evaluated as a tool for metabolite profiling of the *Escherichia coli* (*E. coli*) metabolome, which, according to the authors, comprised hydrophobic lipids, inorganic ions, volatile alcohols and ketones, amino and non-amino organic acids, and hydrophilic carbohydrates (Dwivedi et al., 2008). From >500 features detected, >200 could be assigned as *E. coli* metabolites.

C. Bioinformatics and Chemometrics

Perhaps the most important, albeit one of the most difficult, aspects of metabolomic science lies in the choice and use of appropriate chemometric data analysis (Patterson & Idle, 2009). Such data analysis approaches include proper quality control and data-normalization methods as essential, initial steps even before a single biomarker can be identified with multivariate data analysis (MDA). Additional quality-control steps, including analysis of pooled samples, spiked samples, biological and technical replicates, as well as the influence of injection order, are equally important and have been discussed elsewhere (Enot et al., 2008). There exists currently several commercial (e.g., Waters MarkerLynx) as well as public (e.g., XCMS, MZmine, MetAlign) software tools that are useful for data deconvolution, normalization, and quality control (Benton et al., 2008, Katajamaa et al., 2006, Lommen, 2009, Nordstrom et al., 2006, Smith et al., 2006). In terms of radiation metabolomics, MarkerLynx and MZmine have both been deployed successfully to identify radiation biomarkers using UPLC-ESI-QTOFMS and GC-MS platforms, respectively (Lanz et al., 2009, Patterson et al., 2008, Tyburski et al., 2008, Tyburski et al., 2009). Peak picking, retention-time correction, total spectral normalization and filtering, and missing-value interrogation are some important features when choosing deconvolution software. Additional considerations include the extent to which the end-user wishes to control and fine-tune each parameter because some platforms allow for more (e.g., XCMS or MZmine) or less (e.g., MarkerLynx) control over the deconvolution process.

Methods for metabolomic-data analysis have been reviewed extensively, and are well-documented and discussed in the literature (Dettmer, et al., 2007, Patterson & Idle, 2009). Here, we wish to briefly review some of the more-common place approaches, and to introduce two new approaches, Random Forests and self-organizing maps (SOMs) that have found great functionality in radiation metabolomic studies.

1. PCA, PLS-DA, OPLS, and Random Forests—A quick review of the metabolomics literature reveals an overwhelming preference for dimension-reduction methods to model and visualize ^{1}H NMR, GC-MS, and LC-MS data. Such methods include principal components analysis (PCA), projection to latent structures discriminant analysis (PLS-DA), and more recently, orthogonal projection to latent structures (OPLS) (Trygg et al., 2007,

Trygg & Wold, 2002). These methods, of course, are well-suited for the high-dimensionality often found with mass spectrometry-based data, and useful information can be gleaned from the scores plots (e.g., outlier identification, sample clustering) and the loadings plots (e.g., important variables) (Castle et al., 2006). Recently, introduction of the S-plot, which utilizes measures of model fit or reliability (p(corr)1 in SIMCA-P+, Umetrics) and covariance (p1) to generate an "S"-shaped plot, has found exceptional utility to clearly display depleted and enriched biomarkers (Wiklund et al., 2008). In other words, this plot accentuates and "pulls" potentially important variables from the cloud of variables found in typical loadings plots.

Although the usefulness of those methods is indisputable, a few words of caution are worth mentioning. Scaling of data (mean centering, unit variance, or Pareto) can introduce unwanted and unintended consequences especially modeling of noise or overfitting the data; thus, proper and extensive data validation is required (Bottcher et al., 2008, Westerhuis et al., 2008). That problem is compounded by that fact that metabolomic datasets typically have a small sample size, but a large number of variables (i.e., small n, large p problem). Additionally, because metabolome constituents can have considerably different concentrations, and hence considerably different variances from sample to sample, methods dependent on covariance might be insensitive to identify biochemicals of relatively low abundance (with smaller changes in variance).

As a complimentary approach to methods such as PCA or OPLS, the machine-learning algorithm Random Forests (Breiman, 2001) was implemented into our chemometric workflow (Lanz, et al., 2009, Tyburski, et al., 2009) because it can handle well high-dimension data, operates independent of data scale, and provides a convenient and robust measurement of misclassification error (Barrett & Cairns, 2008, Enot et al., 2006, Enot, et al., 2008, Heidema & Nagelkerke, 2008, Wu et al., 2003). Random Forests is freely available, and can be used in the R software environment (http://cran.r-project.org/). It is based on the classification and regression tree (CART) method, and uses an ensemble of decision trees to build a highly accurate classifier. Important tunable parameters include *ntree*, the number of trees grown, and *mtry*, the number of variables sampled at each split. The variable-importance measure (and Gini index) provides a list of variables that is ranked beginning with the most important. Multidimensional scaling (MDS) plots using the proximity matrix (a valuable feature of the Random Forests algorithm) can be used to display graphically similarities and dissimilarities in the samples. In other words, sample relationships existing in the high dimensional datasets are displayed graphically in, typically, a two-dimensional space. Furthermore according to Breiman (http://www.stat.berkeley.edu/~breiman/RandomForests/cc_home.htm), and one of its most important features, Random Forests might be less likely to overfit data.

As further evidence of its potential utility in metabolomic investigations, Random Forests is included as a chemometric tool on several websites that are dedicated to metabolomic data analysis. Examples include MetaboAnalyst (http://www.metaboanalyst.ca) (Xia et al., 2009) and MetaFIND (http://mlg.ucd.ie/metafind) (Bryan et al., 2008) that provide convenient interfaces, that require little or no knowledge of the R software environment.

2. Gene Expression Dynamics Inspector (GEDI)—When compared to the genome and proteome, the metabolome is poorly annotated. Even with concerted efforts by the Human Metabolome Database (HMDB) (Forsythe & Wishart, 2009, Wishart et al., 2009, Wishart et al., 2007) and the LIPID metabolites and pathways strategy (LIPID MAPS) Consortium (Fahy et al., 2007, Sud et al., 2007) to identify the many biochemical constituents that make up the metabolome (or lipidome), there still remains a considerable gap of knowledge about the make-up, concentration, and flux of biochemicals in biofluids, cells, and tissues. As already discussed, the study and measurement of the metabolome is

platform- and context-dependent; thus, the metabolome annotation task is an arduous and expensive undertaking.

Unlike GC-MS, which matches spectra against the comprehensive NIST database, metabolomics platforms based on LC-MS often do not have such a luxury. Standard LC-MS libraries are uncommon due to myriad reasons, including non-standardized liquid chromatography conditions, differences in ion measurement and detection, as well as a general lack of spectral databases based on specific ionization methods such as ESI. Consequently, LC-MS-based metabolomic investigations often identify “anonymous” biomarkers; that is, they are identified only by an *m/z* and retention time value. Metabolomics, of course, must not be confused with metabolic profiling, in which specific, known biochemical constituents are profiled to thus avoid this conundrum. However, the technique described below applies equally to metabolic profiling assays, and is likely to be of value in metabolic profiling applications.

Despite the lack of chemical identities reported from LC-MS metabolomics investigations, it is useful for the aforementioned reasons to present these data in a visually intuitive and appealing manner. For example, hierarchical clustering can be used to highlight differences between groups in a manner that is similar to methods often used to display gene-expression data. Information presented in this manner, however, is biochemical-centric and does not easily convey a holistic view of the metabolomic response at the sample or system level. The Gene Expression Dynamics Inspector (GEDI) (http://www.childrenshospital.org/research/ingber/GEDI/gedihome.htm), which was originally designed for gene expression analysis and is based on the self-organizing map algorithm (SOM), is useful to present complex and anonymous LC-MS-acquired metabolomics data so that simple comparisons can be quickly and easily made. Unlike heat maps, SOMs reduce dataset complexity by clustering metabolites that share similar abundance patterns across the dataset (Fig. 1). GEDI has been used to display holistic views of the cellular and mouse urinary radiation-responsive metabolomes (Patterson, et al., 2008, Tyburski, et al., 2008). As a further example of a GEDI application to metabolome visualization, changes in the rat urinary metabolome (measured with GC-MS) were visualized (Fig. 2A–B). Clusters of depleted and enriched ions are easily observed in the averaged and individual GEDI mosaics. In general, a portion of the radiation-responsive urinary metabolome can be thought of as cool (indicated by tiles that change from deep red in the sham to dark blue in the irradiated) or hot (indicated by tiles that change from dark blue in the sham to deep red in the irradiated). Radiation-responsive ions include those derived from phosphate, lactic acid, and uracil, for example (see below). Similar approaches based on the SOM algorithm have also been reported (Akiyama et al., 2008, Hirai et al., 2005, Hirai et al., 2004, Makinen et al., 2008). Although not very efficient for in-depth biomarker investigations, methods based on the SOM algorithm such as GEDI might ultimately be deployed as a visual means of pattern recognition to quickly differentiate samples.

D. Biomarker Discovery in Radiation Metabolomics

The basic protocol that has been used to date in radiation metabolomics is depicted in Fig. 3. In all cases, γ-irradiated animals or cell cultures were compared to sham-irradiated (control) animals or cells. UPLC-ESI-QTOFMS and GC-MS analyses have both provided data matrices that were then deconvoluted and subjected to multivariate data analysis and/or Random Forests analysis to yield biomarkers of γ irradiation. Biomarkers identified by UPLC-ESI-QTOFMS were then accurately quantitated using an ABI2000 triple-quadrupole (multiple reaction monitoring) to address concerns of the limited dynamic range associated with QTOF instruments. Dose-response relationships were examined with the GEDI SOM algorithm. Furthermore, preliminary studies by our colleagues at Sionex Corporation, with IMS in the configuration of atmospheric pressure ionization (API) and differential mobility

spectrometry (DMS) as ion prefiltration for mass spectrometry, have demonstrated the potential to develop a miniaturized device to detect radiation metabolomic signatures in the field (Nazarov et al., 2008).

1. The radiation metabolomic signature – proof of concept in γ-irradiated mice —Our preliminary investigation (Tyburski, et al., 2008) used mice that had been γ-irradiated at doses of 3, 6, 7, 8, and 11 Gy. Urines (0–24h) collected from mice that were acclimated to metabolic cages on days −6, −4, and −2, and exposed to 3 and 8 Gy, were used for radiation biomarker mining with UPLC-QTOFMS in ESI- mode. Data matrices were subjected to multivariate data analysis with OPLS, and the potential biomarkers were selected by eye from the OPLS S-plots (Fig. 4). Figs. 4A and 4B clearly show that the OPLS model resolved the 3 Gy and 8 Gy γ-irradiated mice from the sham controls. The resulting loadings plots (Figs. 4C and 4D) display the ions that contribute to these differences between irradiated and sham-irradiated mice with a measure of fit to the OPLS model on the ordinate and a measure of ion abundance on the abscissa. Because mass errors were ca. 0–4 ppm, it was possible to derive empirical formulae for a number of ions, their in-source fragments, and +1 isotopes. Comparison with authentic standards yielded the following radiation biomarkers (dose) in mouse urine: 3-hydroxy-2-methylbenzoic acid *O*-sulfate (3 Gy), *N*-hexanoylglycine (3 and 8 Gy), citric acid/isocitric acid (3 and 8 Gy), β-thymidine (3 and 8 Gy), and taurine (8 Gy). In addition, creatinine, which was used to normalize ion abundances instead of urine volume, was also elevated at 8 Gy. The enhanced urinary excretion of radiation biomarkers is shown in Fig. 5. Thus, the use of UPLC-QTOFMS in ESI- mode detected and defined a radiation metabolomic signature in mouse urine at 3 and 8 Gy radiation doses, which are roughly equivalent to human doses of 1.7 and 4.6 Gy, respectively. These radiation exposures in human populations would be expected to be below and within the range (2.5–5 Gy) considered to be associated with the radiation hematopoietic syndrome (Hall & Giaccia, 2006).

2. The Radiation Metabolomic Dose-Response – Proof of Concept with GEDI—Although there existed preliminary evidence (Fig. 5) of an effect of radiation dose (3 and 8 Gy) on the metabolomic response as revealed by UPLC-ESI-QTOFMS, GEDI was used to examine the patterns of metabolite excretion at 0, 6, 7, 8, and 11 Gy in order to obtain a more global and comprehensive snapshot of metabolite changes (Tyburski, et al., 2008). As described above, GEDI organizes the data matrix into tiles, where each tile contains ions that vary similarly across the sample set, and for which deep-red indicates enriched ions, through shades of orange, yellow and green to deep blue, which indicate depleted ions (see also Fig. 1). Fig. 6A displays the gradual change for the ESI- mode in the GEDI map from 0 to 11 Gy. As can be seen, there is a gradual shrinking of a large cluster of “hot” tiles as the radiation dose is gradually increased. A 3×3 matrix of nine tiles in the bottom-left of the map also “cools”, and this cooling can be clearly seen in Fig. 6B when the data are expressed in the form of a dose-response curve. Moreover, another 3×3 matrix of nine tiles in the bottom-right corner of the map gradually heats up in response to an increased radiation dose, and this heating can be clearly seem in Fig. 6C. Finally Fig. 6D displays the change in ESI+ mode for which a dose-response effect is also clearly visible. Therefore, the application of UPLC-ESI-QTOFMS to the analysis of urine of γ-irradiated mice has demonstrated not only a qualitative, but also a quantitative, radiation metabolomic signature.

3. Mechanistic Underpinnings of the Radiation Metabolomic Signature—The preliminary studies to yield proof of concepts provided few mechanisms by which radiation produced a metabolomic signature. A better understanding of this process would assist research on many fronts, including efforts to prevent or ameliorate radiation damage. Further studies were carried out in mice, this time at sublethal doses of 1–3 Gy (Tyburski, et

al., 2009). Again, UPLC-ESI-QTOFMS was employed for urine analysis in ESI+ and ESI- modes. In addition to MDA by OPLS, the data matrix was subjected to Random Forests analysis. Inspection of the top 150 enriched and depleted ions at each radiation dose determined with Random Forests (25 iterations with bootstrapping) revealed an intriguing pattern, as shown in a Venn diagram (Fig. 7A). It can be seen that a similar number of ions is shared between one radiation dose and either of the other two doses (13–19 ions) and that a total of 25 of the top 150 enriched ions at each dose are common among all three doses. These are the biomarkers of greatest interest. From within these ions, a pattern emerges, that three deoxynucleosides, specifically, 2'-deoxyxanthosine, thymidine, and 2'-deoxyuridine, were ranked 1st, 3rd, and 4th, respectively, by Random Forests. Xanthine and xanthosine were also identified (Fig. 7B). But, *N*-hexanoylglycine, which had been reported as a biomarker of 3 and 8 Gy exposure (Tyburski, et al., 2008), was ranked only #1146 by Random Forests in this subsequent study (Tyburski, et al., 2009). Comparison of the two methods reveals the discrepancy, that *N*-hexanoylglycine (marker #2) has the poorest correlation (0.5–0.6) to the OPLS model (Figs. 4C and 4D) of all the chosen biomarkers. This underscores the unbiased nature of the Random Forests analysis *versus* the OPLS analysis whereby human judgment might lead to erroneous conclusions as in the case of OPLS and *N*-hexanoylglycine.

Again, clear evidence of a dose-response effect of γ-irradiation on the mouse urinary metabolome was found. Fig. 8 shows the dose-response relationship for thymidine and 2'-deoxyuridine. Interestingly, excretion of 2'-deoxycytidine decreased after 2 and 3 Gy doses (Fig. 8E and 8F). 2'-Deoxycytidine is an aminonucleoside, which when oxidized by cytidine deaminase (EC 3.5.4.5) yields 2'-deoxyuridine, with the amino group replaced by a tautomeric hydroxy/keto group. Thymidine is also a non-amino 2'-deoxynucleoside. Based upon these, and other, considerations, it was concluded that γ-radiation leads to the formation of reactive oxygen and nitrogen species (ROS and RNS) in the mouse, and that nitrous anhydride (N_2O_3) thus formed participates in nitrosative deamination of purines and pyrimidines (Tyburski, et al., 2009). It is worthy of note that all the validated and enriched biomarkers (Fig. 7B) that comprise the radiation metabolomic signature in mouse urine are deaminated purines and pyrimidines.

4. Persistence of the Radiation Metabolomic Signature in Mouse Urine—An important practical issue in the field will be the persistence of the metabolomic signature. Although it is most useful to screen populations within 24 h of a nuclear or radiological environmental incident, a longer-lasting footprint of radiation damage might also have its utility. Accordingly, the time course of the urinary excretion of radiation biomarkers was studied in detail with the collection of 4-h urine samples. Fig. 9 shows that the two deaminated pyrimidine biomarkers, thymidine and 2'-deoxyuridine, peak in their excretion at 8 h, and by 4 days have virtually disappeared; those data indicate a transient urinary radiation response. This phenomenon is worthy of further investigation in other species, including Man.

5. Proof of Concept in a Second Species – The Rat—As a first step to determine species-specificity of the radiation metabolomic signature, studies have been performed in the rat (Lanz, et al., 2009). A different approach to the mouse studies already described (Tyburski, et al., 2008, Tyburski, et al., 2009) was adopted. First, rats were kept continuously in metabolic cages for 4 days prior to irradiation/sham irradiation, and daily urines were collected. After γ-irradiation with 3 Gy, rats were returned to their metabolic cages for a further continuous 3 days, with daily urine collections. In addition, water (ml) and food consumption (g), together with body weight (g) and urine volume (ml/24 h), were all recorded for test and control animals. Daily urinary excretion (μmol/24 h) of Na^+, K^+, Ca^{2+}, Cl^-, PO_4^{3-}, and urea were also recorded. Because of highly significant changes in

some of these parameters that occurred after irradiation, additional experiments were undertaken to examine the effect of 24-h food deprivation and to eliminate or confirm any possibility that these changes were due to the grossly reduced food intake that followed irradiation of the rats. All data indicate that the effects observed are largely radiation-specific.

Urines were analyzed with GC-MS after derivatization with methoxyamine hydrochloride followed by silylation with BSTFA/TMCS. Chromatogram alignment was done with MZmine, and the resultant peak table was analyzed by Random Forests only. The principal upregulated biomarkers in rat urine were inorganic phosphate, glyoxylic acid, threonic acid, thymine, uracil, cytosine, glycerol 3-phosphate, and *p*-cresol; however, glycerol 3-phosphate appears to be due largely to reduced excretions in the sham irradiated rats (Fig. 10). Of greatest interest was the observation that, within 24 h of irradiation, but not subsequently, there was an elevated urinary excretion of thymine and uracil. It should be stated here that neither nucleosides nor 2'-deoxynucleosides were detected in rat urine samples. Furthermore, it was demonstrated that thymidine was converted to thymine under the assay conditions by deribosylation during the derivatization reactions and that 2'-deoxyuridine and 2'-deoxycytidine were also deribosylated to uracil and cytosine, respectively. Therefore, the observation of elevated urinary excretion of both thymine and uracil in rats irradiated with 3 Gy would appear to confirm the observations of thymidine and 2'-deoxyuridine as principal radiation biomarkers in the mouse. As previously discussed (Lanz, et al., 2009), other biomarkers such as glyoxylic acid and threonic acid almost certainly arise from the intervention of ROS; that factor also adds weight to the interpretation of the mouse data (Tyburski, et al., 2009). Finally, it should be noted that, after an initial increase, the urinary excretion by irradiated rats of cytosine fell almost to zero (Fig. 10E). It was also demonstrated that 2'-deoxycytidine was deribosylated to cytosine in the sample-derivatization process (Lanz, et al., 2009). Again, this finding would seem to fit well with the observation in mice of a reduced excretion of 2'-deoxycytidine (Tyburski, et al., 2009). Thus, proof of concept in a second species was accomplished.

6. Studies of the Radiation Metabolomic Signature at a Cellular Level—In order to understand better the effect of γ radiation on cellular metabolomes, and to gain further insight into the mechanisms behind the response, UPLC-ESI-QTOFMS was used to profile water-soluble metabolites from lysates of human B lymphoblastoid TK6 cells and human BJ fibroblasts that had been γ-irradiated with doses from 0.5 to 8 Gy (Patterson, et al., 2008). Multivariate data analysis was carried out with PLS-DA, which revealed clustering and resolution of the sham, 0.5 Gy, 1.0 Gy, 4.0 Gy, and 8 Gy doses in the PLS-DA scores plot 1 h after irradiation. Apart from the 8 Gy cluster, scores for the other doses began to merge between 4 and 8 h after irradiation of TK6 cells. For the BJ fibroblast cell line, the scores for sham, 1.0 Gy, and 4.0 Gy remained distinct over the full 16-h of the experiment. A PLS-DA loadings S-plot revealed a significant number of ions that arose from cellular constituents that were clearly attenuated after irradiation, even at only 1 Gy. Empirical formulae corresponded to reduced glutathione (GSH), adenosine monophosphate (AMP), and their fragment ions. The attenuation of GSH after radiation is a clear sign of the generation of ROS, and supports the *in vivo* studies described above. AMP is a principal nucleoside monophosphate derived from the aminonucleoside adenosine. The *in vivo* observations strongly suggest attrition of aminonucleosides, purines and pyrimidines (Tyburski, et al., 2009), and these data of reduced AMP support the mouse observations. However, there could be many other explanations for the reduction in cellular AMP after ionizing radiation. Interestingly, there has appeared a recent report of irradiation of human fibroblasts with 10 Gy followed by proteomic analysis of cell lysates (Hu et al., 2008). As reviewed in Table 2, many enzymes were either up- or down-regulated, including AMP. In all cases, the proteomic and metabolomic findings were reconcilable.

UPLC-ESI-QTOFMS studies of cellular metabolomes *in vitro* appear to provide a useful adjunct to *in vitro* proteomic studies of radiation response and *in vivo* investigations of ionizing radiation.

V. FIELD INSTRUMENTATION AND PERSPECTIVE

As stated above, there is an urgent need to develop high-throughput minimally-invasive radiation-biomonitoring devices in the event of a terrorist or accidental nuclear or radiological event that would affect a large population. Time-to-emesis seems to be the current and most reliable early indicator of dose. Contemporary science should be able to deliver a more objective measure, one that can be packaged into a portable device that can be added to the national stockpile. Only a few years ago, the idea that there could be a radiation metabolomic signature that might have utility to estimate exposure doses in human populations was considered fanciful. We have now in hand the proof of concept that there is a discernable radiation metabolomic signature that is qualitative and quantitative in nature. Of course, much more research and development is needed, in particular into metabolomes other than urine, that would be those most readily accessible to first responders and/or those with minimal training. Here, we have in mind sebum, perhaps from swabbing facial skin, or cerumen removed from the ear, or possibly saliva. The advantage of the more lipophilic metabolomes is that the ionizing radiation metabolomic signature might be more long-lived than that derived from urine. Of paramount importance will be studies in humans that, in principle, could be performed in patients who would undergo whole-body or partial-body radiation therapy. However, human metabolomic studies are notoriously difficult to perform, if only because of potential confounding factors (e.g., genetic and dietary diversity, (Lawton, et al., 2008), and concomitant chemotherapy). Extensive human studies are required in order to catalog the composition of the various metabolomes as well as to establish metabolomic baselines from which to measure significant deviations due to radiation exposure. Furthermore, understanding the influence of factors such as age, diet, gender, locale, and lifestyle is important, if not essential, for biomarkers derived from metabolomic investigations to transition into the field.

If the radiation metabolomic successes accomplished in laboratory rodents and cell cultures translate to humans, then the remaining task is merely a problem of engineering. In our limited experience, it is likely that this engineering solution will involve some form of IMS device–one that can be miniaturized and interfaced with simple electrospray and mass-selective detection components. Such a hybrid instrument could also find considerable utility in clinical practice and in radiation protection in the workplace.

The remarkable nature of mass spectrometry has brought us to the threshold of a new age, where the screening of wide-scale populations for early signs of radiation sickness might actually become a reality.

Acknowledgments

This work was funded by NIH (NIAID) Grant U19 AI067773-02 and the National Cancer Institute, Intramural Research Program, Center for Cancer Research. A.D.P. was supported by a Pharmacology Research Associate in Training Fellowship from the National Institute of General Medical Sciences. J.R.I. is grateful to U.S. Smokeless Tobacco Company for a Grant for collaborative research.

Abbreviations

LC-MS	liquid chromatography-coupled mass spectrometry
GC-MS	gas chromatography-coupled mass spectrometry

UPLC	ultra-performance liquid chromatography
MDA	multivariate data analysis
MDS	multidimensional scaling plot
PCA	principal components analysis
PLS-DA	projection to latent structures discriminant analysis
OPLS	orthogonal projection to latent structures
IR	ionizing radiation
m/z	mass-to-charge ratio

References

Akiyama K, Chikayama E, Yuasa H, Shimada Y, Tohge T, Shinozaki K, Hirai MY, Sakurai T, Kikuchi J, Saito K. PRIMe: a Web site that assembles tools for metabolomics and transcriptomics. In Silico Biol. 2008; 8:339–345. [PubMed: 19032166]

Amundson SA, Bittner M, Meltzer P, Trent J, Fornace AJ Jr. Biological indicators for the identification of ionizing radiation exposure in humans. Expert Rev Mol Diagn. 2001; 1:211–219. [PubMed: 11901816]

Amundson SA, Bittner M, Meltzer P, Trent J, Fornace AJ Jr. Induction of gene expression as a monitor of exposure to ionizing radiation. Radiat Res. 2001; 156:657–661. [PubMed: 11604088]

Amundson SA, Do KT, Fornace AJ Jr. Induction of stress genes by low doses of gamma rays. Radiat Res. 1999; 152:225–231. [PubMed: 10453082]

Amundson SA, Do KT, Shahab S, Bittner M, Meltzer P, Trent J, Fornace AJ Jr. Identification of potential mRNA biomarkers in peripheral blood lymphocytes for human exposure to ionizing radiation. Radiat Res. 2000; 154:342–346. [PubMed: 11012342]

Amundson SA, Fornace AJ Jr. Gene expression profiles for monitoring radiation exposure. Radiat Prot Dosimetry. 2001; 97:11–16. [PubMed: 11763352]

Amundson SA, Fornace AJ Jr. Monitoring human radiation exposure by gene expression profiling: possibilities and pitfalls. Health Phys. 2003; 85:36–42. [PubMed: 12852469]

Barrett JH, Cairns DA. Application of the random forest classification method to peaks detected from mass spectrometric proteomic profiles of cancer patients and controls. Stat Appl Genet Mol Biol. 2008; 7 Article4.

Benton HP, Wong DM, Trauger SA, Siuzdak G. XCMS2: processing tandem mass spectrometry data for metabolite identification and structural characterization. Anal Chem. 2008; 80:6382–6389. [PubMed: 18627180]

Blakely WF, Carr Z, Chu MC, Dayal-Drager R, Fujimoto K, Hopmeir M, Kulka U, Lillis-Hearne P, Livingston GK, Lloyd DC, Maznyk N, Perez Mdel R, Romm H, Takashima Y, Voisin P, Wilkins RC, Yoshida MA. WHO 1st consultation on the development of a global biodosimetry laboratories network for radiation emergencies (BioDoseNet). Radiat Res. 2009; 171:127–139. [PubMed: 19138057]

Blakely WF, Salter CA, Prasanna PG. Early-response biological dosimetry--recommended countermeasure enhancements for mass-casualty radiological incidents and terrorism. Health Phys. 2005; 89:494–504. [PubMed: 16217193]

Bottcher C, Centeno D, Freitag J, Hofgen R, Kohl K, Kopka J, Kroymann J, Matros A, Mock HP, Neumann S, Pfalz M, von Roepenack-Lahaye E, Schauer N, Trenkamp S, Zubriggen M, Fernie AR. Teaching (and learning from) metabolomics: the 2006 PlantMetaNet ETNA Metabolomics Research School. Physiol Plant. 2008; 132:136–149. [PubMed: 18251856]

Breiman L. Random Forests. Machine Learning. 2001; 45:5–32.

Bryan K, Brennan L, Cunningham P. MetaFIND: a feature analysis tool for metabolomics data. BMC Bioinformatics. 2008; 9:470. [PubMed: 18986526]

Castle AL, Fiehn O, Kaddurah-Daouk R, Lindon JC. Metabolomics Standards Workshop and the development of international standards for reporting metabolomics experimental results. Brief Bioinform. 2006; 7:159–165. [PubMed: 16772263]

Chumak VV. Physical dosimetry of Chernobyl cleanup workers. Health Phys. 2007; 93:452–461. [PubMed: 18049221]

Coen M, Holmes E, Lindon JC, Nicholson JK. NMR-based metabolic profiling and metabonomic approaches to problems in molecular toxicology. Chem Res Toxicol. 2008; 21:9–27. [PubMed: 18171018]

Graham, B.; Talent, JM.; Allison, GT. World at risk the report of the Commission on the Prevention of WMD Proliferation and Terrorism. New York: Vintage Books; 2008. Commission on the Prevention of Weapons of Mass Destruction Proliferation and Terrorism (U.S.); p. xxviiip. 132

Conklin WC, Liotta PL. Radiological threat assessment and the Federal Response Plan--a gap analysis. Health Phys. 2005; 89:457–470. [PubMed: 16217189]

Dalgliesh CE, Horning EC, Horning MG, Knox KL, Yarger K. A gas-liquid-chromatographic procedure for separating a wide range of metabolites occuring in urine or tissue extracts. Biochem J. 1966; 101:792–810. [PubMed: 16742460]

Dettmer K, Aronov PA, Hammock BD. Mass spectrometry-based metabolomics. Mass Spectrom Rev. 2007; 26:51–78. [PubMed: 16921475]

Dorr HD, Meineke V. Appropriate radiation accident medical management: necessity of extensive preparatory planning. Radiat Environ Biophys. 2006; 45:237–244. [PubMed: 17047978]

Duarte IF, Legido-Quigley C, Parker DA, Swann JR, Spraul M, Braumann U, Gil AM, Holmes E, Nicholson JK, Murphy GM, Vilca-Melendez H, Heaton N, Lindon JC. Identification of metabolites in human hepatic bile using 800 MHz 1H NMR spectroscopy, HPLC-NMR/MS and UPLC-MS. Mol Biosyst. 2009; 5:180–190. [PubMed: 19156264]

Dwivedi P, Wu P, Klopsch SJ, Puzon GJ, Xun L, Hill HH Jr. Metabolic profiling by ion mobility mass spectrometry (IMMS). Metabolomics. 2008; 4:63–80.

Eisenreich W, Bacher A. Advances of high-resolution NMR techniques in the structural and metabolic analysis of plant biochemistry. Phytochemistry. 2007; 68:2799–2815. [PubMed: 18023829]

Ellis DI, Dunn WB, Griffin JL, Allwood JW, Goodacre R. Metabolic fingerprinting as a diagnostic tool. Pharmacogenomics. 2007; 8:1243–1266. [PubMed: 17924839]

Eneroth P, Gordon B, Ryhage R, Sjovall J. Identification of mono- and dihydroxy bile acids in human feces by gas-liquid chromatography and mass spectrometry. J Lipid Res. 1966; 7:511–523. [PubMed: 5966634]

Enot DP, Beckmann M, Overy D, Draper J. Predicting interpretability of metabolome models based on behavior, putative identity, and biological relevance of explanatory signals. Proc Natl Acad Sci U S A. 2006; 103:14865–14870. [PubMed: 16990432]

Enot DP, Lin W, Beckmann M, Parker D, Overy DP, Draper J. Preprocessing, classification modeling and feature selection using flow injection electrospray mass spectrometry metabolite fingerprint data. Nat Protoc. 2008; 3:446–470. [PubMed: 18323816]

Fahy E, Sud M, Cotter D, Subramaniam S. LIPID MAPS online tools for lipid research. Nucleic Acids Res. 2007; 35:W606–W612. [PubMed: 17584797]

Faustino PJ, Yang Y, Progar JJ, Brownell CR, Sadrieh N, May JC, Leutzinger E, Place DA, Duffy EP, Houn F, Loewke SA, Mecozzi VJ, Ellison CD, Khan MA, Hussain AS, Lyon RC. Quantitative determination of cesium binding to ferric hexacyanoferrate: Prussian blue. J Pharm Biomed Anal. 2008; 47:114–125. [PubMed: 18242038]

Forsythe IJ, Wishart DS. Exploring human metabolites using the human metabolome database. Curr Protoc Bioinformatics Chapter. 2009; 14 Unit14 18.

Goans RE, Waselenko JK. Medical management of radiological casualties. Health Phys. 2005; 89:505–512. [PubMed: 16217194]

Hall, EJ.; Giaccia, AJ. Radiobiology for the radiologist. Philadelphia: Lippincott Williams & Wilkins; 2006.

Heidema AG, Nagelkerke N. Developing a discrimination rule between breast cancer patients and controls using proteomics mass spectrometric data: a three-step approach. Stat Appl Genet Mol Biol. 2008; 7 Article5.

Hirai MY, Klein M, Fujikawa Y, Yano M, Goodenowe DB, Yamazaki Y, Kanaya S, Nakamura Y, Kitayama M, Suzuki H, Sakurai N, Shibata D, Tokuhisa J, Reichelt M, Gershenzon J, Papenbrock J, Saito K. Elucidation of gene-to-gene and metabolite-to-gene networks in arabidopsis by integration of metabolomics and transcriptomics. J Biol Chem. 2005; 280:25590–25595. [PubMed: 15866872]

Hirai MY, Yano M, Goodenowe DB, Kanaya S, Kimura T, Awazuhara M, Arita M, Fujiwara T, Saito K. Integration of transcriptomics and metabolomics for understanding of global responses to nutritional stresses in Arabidopsis thaliana. Proc Natl Acad Sci U S A. 2004; 101:10205–10210. [PubMed: 15199185]

Holmes E, Nicholls AW, Lindon JC, Connor SC, Connelly JC, Haselden JN, Damment SJ, Spraul M, Neidig P, Nicholson JK. Chemometric models for toxicity classification based on NMR spectra of biofluids. Chem Res Toxicol. 2000; 13:471–478. [PubMed: 10858320]

Hu ZZ, Huang H, Cheema A, Jung M, Dritschilo A, Wu CH. Integrated Bioinformatics for Radiation-Induced Pathway Analysis from Proteomics and Microarray Data. J Proteomics Bioinform. 2008; 1:47–60. [PubMed: 19088860]

International Atomic Energy Agency; Chernobyl : looking back to go forward proceedings of an International Conference on Chernobyl : Looking Back to Go Forward … held in Vienna; 6–7 September 2005; Vienna, Austria. International Atomic Energy Agency; 2008.

International Atomic Energy Agency. The Radiological accident in Goiânia. Vienna: International Atomic Energy Agency; 1988.

James AT, Martin AJ. Gas-liquid partition chromatography: the separation and micro-estimation of ammonia and the methylamines. Biochem J. 1952; 52:238–242. [PubMed: 13018213]

James AT, Martin AJ. Gas-liquid partition chromatography; the separation and micro-estimation of volatile fatty acids from formic acid to dodecanoic acid. Biochem J. 1952; 50:679–690. [PubMed: 14934673]

James AT, Martin AJ. Liquid-gas partition chromatography. Biochem J. 1951; 48 vii.

Kanu AB, Dwivedi P, Tam M, Matz L, Hill HH Jr. Ion mobility-mass spectrometry. J Mass Spectrom. 2008; 43:1–22. [PubMed: 18200615]

Kanu AB, Hill HH Jr. Ion mobility spectrometry detection for gas chromatography. J Chromatogr A. 2008; 1177:12–27. [PubMed: 18067900]

Katajamaa M, Miettinen J, Oresic M. MZmine: toolbox for processing and visualization of mass spectrometry based molecular profile data. Bioinformatics. 2006; 22:634–636. [PubMed: 16403790]

Keever, BAD. Monroe, ME: Common Courage Press; 2004. News Zero: The New York Times and the Bomb.

Kind T, Fiehn O. Seven Golden Rules for heuristic filtering of molecular formulas obtained by accurate mass spectrometry. BMC Bioinformatics. 2007; 8:105. [PubMed: 17389044]

Kind T, Scholz M, Fiehn O. How large is the metabolome? A critical analysis of data exchange practices in chemistry. PLoS ONE. 2009; 4:e5440. [PubMed: 19415114]

Lanz C, Patterson AD, Slavik J, Krausz KW, Ledermann M, Gonzalez FJ, Idle JR. Radiation Metabolomics 3: Biomarker Discovery in the Urine of Gamma-Irradiated Rats Using a Simplified Metabolomics Protocol of Gas Chromatography-Mass Spectrometry Combined with Random Forests Machine Learning Algorithm. Radiation Research. 2009 in press.

Lawton KA, Berger A, Mitchell M, Milgram KE, Evans AM, Guo L, Hanson RW, Kalhan SC, Ryals JA, Milburn MV. Analysis of the adult human plasma metabolome. Pharmacogenomics. 2008; 9:383–397. [PubMed: 18384253]

Liu RH, Yang J, Lenigk R, Bonanno J, Grodzinski P. Self-contained, fully integrated biochip for sample preparation, polymerase chain reaction amplification, and DNA microarray detection. Anal Chem. 2004; 76:1824–1831. [PubMed: 15053639]

Lommen A. MetAlign: interface-driven, versatile metabolomics tool for hyphenated full-scan mass spectrometry data preprocessing. Anal Chem. 2009; 81:3079–3086. [PubMed: 19301908]

Makinen VP, Forsblom C, Thorn LM, Waden J, Gordin D, Heikkila O, Hietala K, Kyllonen L, Kyto J, Rosengard-Barlund M, Saraheimo M, Tolonen N, Parkkonen M, Kaski K, Ala-Korpela M, Groop

PH. Metabolic phenotypes, vascular complications, and premature deaths in a population of 4,197 patients with type 1 diabetes. Diabetes. 2008; 57:2480–2487. [PubMed: 18544706]

Melo DR, Lipsztein JL, de Oliveira CA, Bertelli L. 137Cs internal contamination involving a Brazilian accident, and the efficacy of Prussian Blue treatment. Health Phys. 1994; 66:245–252. [PubMed: 8106241]

Mousseau TA, Nelson N, Shestopalov V. Don't underestimate the death rate from Chernobyl. Nature. 2005; 437:1089. [PubMed: 16237420]

Nazarov E, Coy SL, Krylov EV, Brenner DJ, Krausz KW, Tyburski JTADP, Slavik J, Fornace AJ Jr, Gonzalez FJ, Idle JR. 56th ASMS Conference on Mass Spectrometry. Denver, CO, June. 2008:1–5.

Nicholson JK, Lindon JC. Systems biology: Metabonomics. Nature. 2008; 455:1054–1056. [PubMed: 18948945]

Nordstrom A, O'Maille G, Qin C, Siuzdak G. Nonlinear data alignment for UPLC-MS and HPLC-MS based metabolomics: quantitative analysis of endogenous and exogenous metabolites in human serum. Anal Chem. 2006; 78:3289–3295. [PubMed: 16689529]

Park JC, Hong YS, Kim YJ, Yang JY, Kim EY, Kwack SJ, Ryu do H, Hwang GS, Lee BM. A metabonomic study on the biochemical effects of doxorubicin in rats using (1)H-NMR spectroscopy. J Toxicol Environ Health A. 2009; 72:374–384. [PubMed: 19199144]

Patterson, AD.; Idle, JR. A metabolomic perspective of small molecule toxicity. In: Ballantyne, B.; Marrs, TC.; Syversen, T.; Ballantyne, B.; Marrs, TC.; Ballantyne, T.; Syversen, B.; Marrs, TC.; Syversen, Ts, editors. General and Applied Toxicology. John Wiley and Sons; 2009.

Patterson AD, Li H, Eichler GS, Krausz KW, Weinstein JN, Fornace AJ Jr, Gonzalez FJ, Idle JR. UPLC-ESI-TOFMS-based metabolomics and gene expression dynamics inspector self-organizing metabolomic maps as tools for understanding the cellular response to ionizing radiation. Anal Chem. 2008; 80:665–674. [PubMed: 18173289]

Paul S, Amundson SA. Development of gene expression signatures for practical radiation biodosimetry. Int J Radiat Oncol Biol Phys. 2008; 71:1236–1244. [PubMed: 18572087]

Pellmar TC, Rockwell S. Priority list of research areas for radiological nuclear threat countermeasures. Radiat Res. 2005; 163:115–123. [PubMed: 15606315]

Robertson DG. Metabonomics in toxicology: a review. Toxicol Sci. 2005; 85:809–822. [PubMed: 15689416]

Sakharov, A. Memoirs. New York: Alfred A. Knopf; 1990.

Scholz M, Fiehn O. SetupX--a public study design database for metabolomic projects. Pac Symp Biocomput. 2007:69–180.

Schull WJ. The somatic effects of exposure to atomic radiation: the Japanese experience, 1947–1997. Proc Natl Acad Sci U S A. 1998; 95:5437–5441. [PubMed: 9576900]

Serkova NJ, Christians U. Biomarkers for toxicodynamic monitoring of immunosuppressants: NMR-based quantitative metabonomics of the blood. Ther Drug Monit. 2005; 27:733–737. [PubMed: 16404806]

Sine RC, Levine IH, Jackson WE, Hawley AL, Prasanna PG, Grace MB, Goans RE, Greenhill RG, Blakely WF. Biodosimety Assessment Tool: a post-exposure software application for management of radiation accidents. Mil Med. 2001; 166:85–87. [PubMed: 11778449]

Smith CA, Want EJ, O'Maille G, Abagyan R, Siuzdak G. XCMS: processing mass spectrometry data for metabolite profiling using nonlinear peak alignment, matching, and identification. Anal Chem. 2006; 78:779–787. [PubMed: 16448051]

Stephan V. Chernobyl: poverty and stress pose 'bigger threat' than radiation. Nature. 2005; 437:181. [PubMed: 16148902]

Straume T, Amundson SA, Blakely WF, Burns FJ, Chen A, Dainiak N, Franklin S, Leary JA, Loftus DJ, Morgan WF, Pellmar TC, Stolc V, Turteltaub KW, Vaughan AT, Vijayakumar S, Wyrobek AJ. NASA Radiation Biomarker Workshop, September 27–28, 2007. Radiat Res. 2008; 170:393–405. [PubMed: 18763867]

Sud M, Fahy E, Cotter D, Brown A, Dennis EA, Glass CK, Merrill AH Jr, Murphy RC, Raetz CR, Russell DW, Subramaniam S. LMSD: LIPID MAPS structure database. Nucleic Acids Res. 2007; 35:D527–D532. [PubMed: 17098933]

Titus, AC. Bombs in the backyard: atomic testing and American politics. Reno, NV: University of Nevada Press; 2001.

Trygg J, Holmes E, Lundstedt T. Chemometrics in metabonomics. J Proteome Res. 2007; 6:469–479. [PubMed: 17269704]

Trygg J, Wold S. Orthogonal projections to latent structures (O-PLS). J Chemometrics. 2002; 16:119–128.

Tyburski JB, Patterson AD, Krausz KW, Slavik J, Fornace AJ Jr, Gonzalez FJ, Idle JR. Radiation metabolomics. 1. Identification of minimally invasive urine biomarkers for gamma-radiation exposure in mice. Radiat Res. 2008; 170:1–14. [PubMed: 18582157]

Tyburski JB, Patterson AD, Krausz KW, Slavik J, Fornace AJ Jr, Gonzalez FJ, Idle JR. Radiation Metabolomics. 2. Dose- and time-dependent urinary excretion of deaminated purines and pyrimidines after sublethal gamma-radiation exposure in mice. Radiation Research. 2009 in press.

Westerhuis J, Hoefsloot H, Smit S, Vis D, Smilde A, van Velzen E, van Duijnhoven J, van Dorsten F. Assessment of PLSDA cross validation. Metabolomics. 2008; 4:81–89.

Wheatley VR, James AT. Studies of sebum. 7. The composition of the sebum of some common rodents. Biochem J. 1957; 65:36–42. [PubMed: 13403868]

Wiklund S, Johansson E, Sjostrom L, Mellerowicz EJ, Edlund U, Shockcor JP, Gottfries J, Moritz T, Trygg J. Visualization of GC/TOF-MS-based metabolomics data for identification of biochemically interesting compounds using OPLS class models. Anal Chem. 2008; 80:115–122. [PubMed: 18027910]

Wishart DS, Knox C, Guo AC, Eisner R, Young N, Gautam B, Hau DD, Psychogios N, Dong E, Bouatra S, Mandal R, Sinelnikov I, Xia J, Jia L, Cruz JA, Lim E, Sobsey CA, Shrivastava S, Huang P, Liu P, Fang L, Peng J, Fradette R, Cheng D, Tzur D, Clements M, Lewis A, De Souza A, Zuniga A, Dawe M, Xiong Y, Clive D, Greiner R, Nazyrova A, Shaykhutdinov R, Li L, Vogel HJ, Forsythe I. HMDB: a knowledgebase for the human metabolome. Nucleic Acids Res. 2009; 37:D603–D610. [PubMed: 18953024]

Wishart DS, Tzur D, Knox C, Eisner R, Guo AC, Young N, Cheng D, Jewell K, Arndt D, Sawhney S, Fung C, Nikolai L, Lewis M, Coutouly MA, Forsythe I, Tang P, Shrivastava S, Jeroncic K, Stothard P, Amegbey G, Block D, Hau DD, Wagner J, Miniaci J, Clements M, Gebremedhin M, Guo N, Zhang Y, Duggan GE, Macinnis GD, Weljie AM, Dowlatabadi R, Bamforth F, Clive D, Greiner R, Li L, Marrie T, Sykes BD, Vogel HJ, Querengesser L. HMDB: the Human Metabolome Database. Nucleic Acids Res. 2007; 35:D521–D526. [PubMed: 17202168]

Wu B, Abbott T, Fishman D, McMurray W, Mor G, Stone K, Ward D, Williams K, Zhao H. Comparison of statistical methods for classification of ovarian cancer using mass spectrometry data. Bioinformatics. 2003; 19:1636–1643. [PubMed: 12967959]

Xia J, Psychogios N, Young N, Wishart DS. MetaboAnalyst: a web server for metabolomic data analysis and interpretation. Nucleic Acids Res. 2009

Xiang Y, Liu Y, Lee ML. Ultrahigh pressure liquid chromatography using elevated temperature. J Chromatogr A. 2006; 1104:198–202. [PubMed: 16376355]

Yang Y, Faustino PJ, Progar JJ, Brownell CR, Sadrieh N, May JC, Leutzinger E, Place DA, Duffy EP, Yu LX, Khan MA, Lyon RC. Quantitative determination of thallium binding to ferric hexacyanoferrate: Prussian blue. Int J Pharm. 2008; 353:187–194. [PubMed: 18226478]

Yushmanov VE. Evaluation of radiation injury by 1H and 31P NMR of human urine. Magn Reson Med. 1994; 31:48–52. [PubMed: 8121268]

Zerhouni E. Medicine. The NIH Roadmap. Science. 2003; 302:63–72. [PubMed: 14526066]

Zoellner, T. Uranium. New York: Viking; 2009.

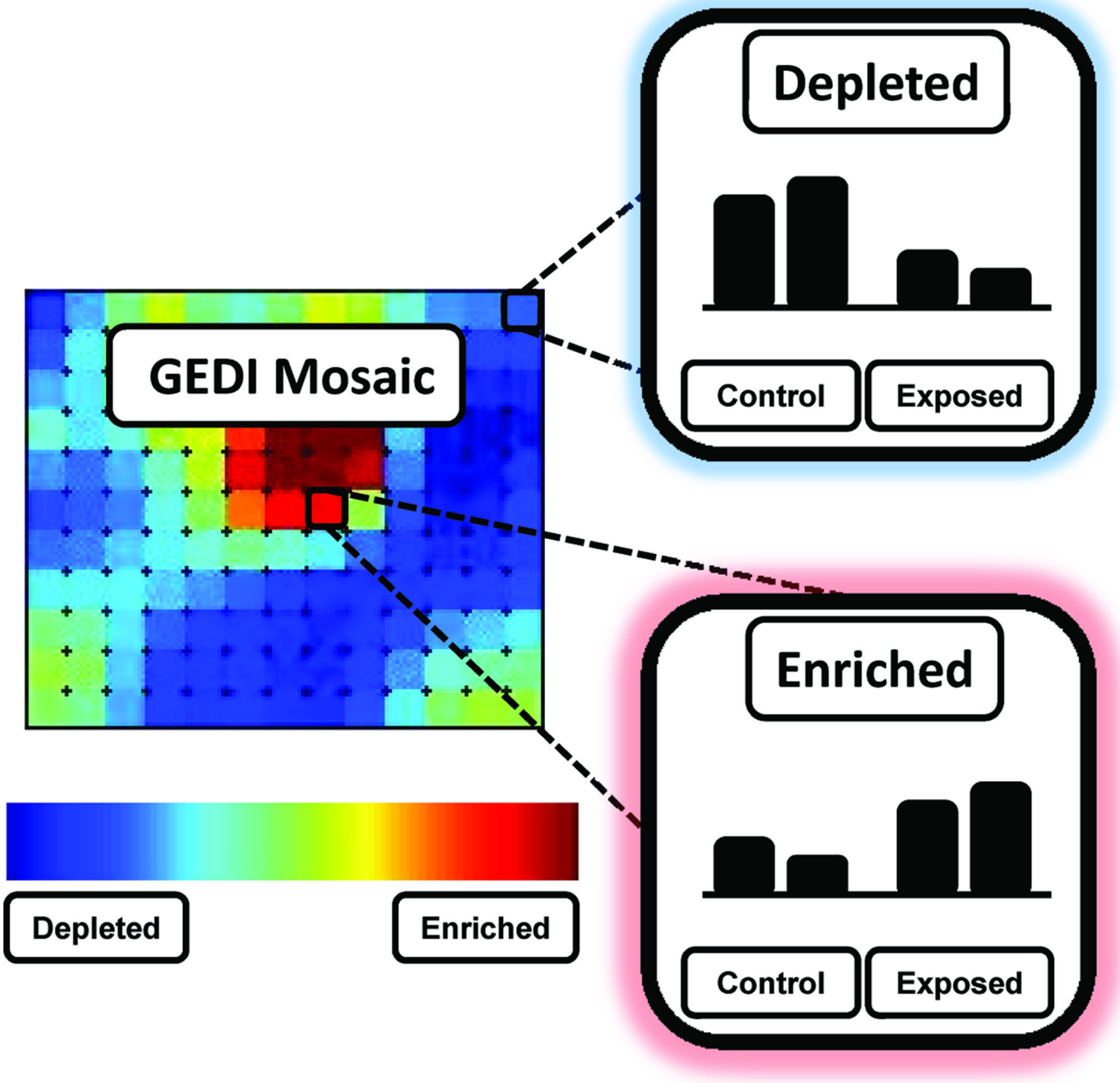

Figure 1.
A typical mosaic generated with Gene Expression Dynamics Inspector (GEDI) of urinary metabolomics data acquired with UPLC-ESI-QTOFMS. GEDI is based on the self-organizing map algorithm, and clusters metabolites that share similar profiles across a dataset into the same tile. Shades of deep blue indicate depleted metabolites, whereas shades of green to yellow to deep red represent increasingly enriched metabolites.

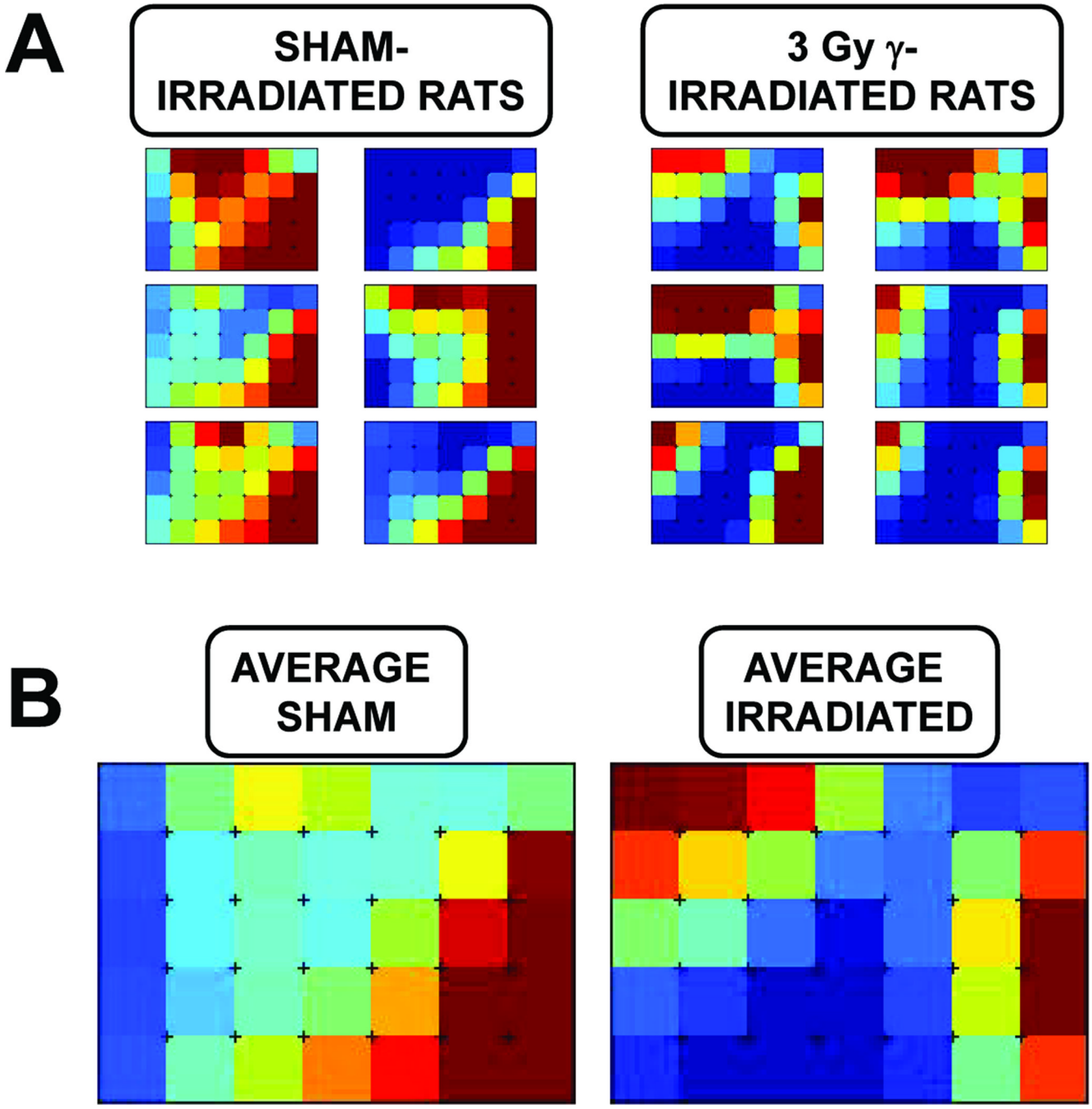

Figure 2.

GEDI can be used to visualize GC-MS data. Sham- and 3 Gy γ-irradiated rat urine was profiled with EI GC-MS, deconvoluted with MZmine, and visualized with GEDI. Individual (A) and averaged (B) mosaics display metabolomic cold and hot spots that are associated with changes in urinary constituents such as phosphate, lactic acid, and uracil.

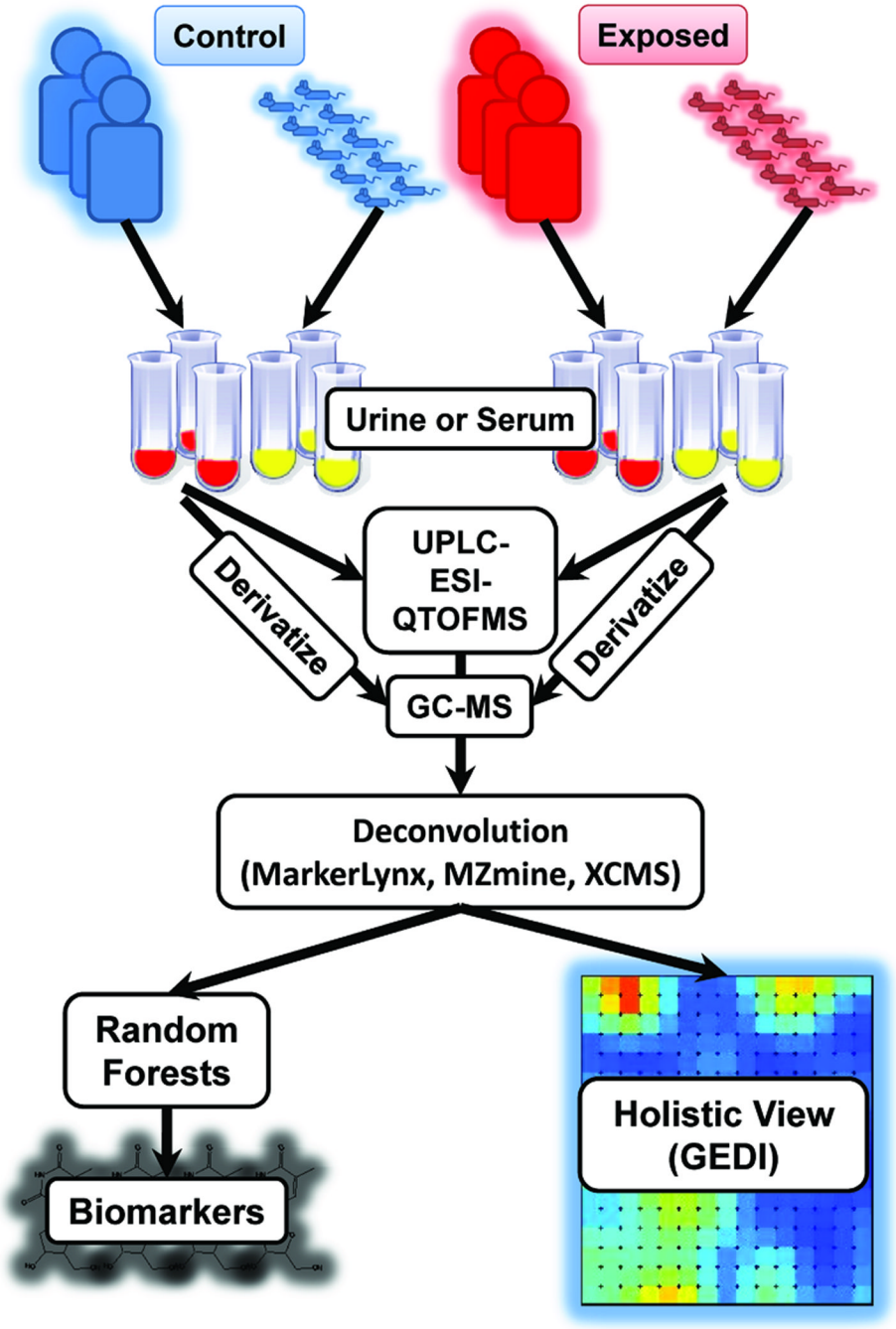

Figure 3.
A flow-chart of the collection of urine or serum from control or exposed, and processing with UPLC-ESI-QTOFMS or GC-MS; sample derivatization is required for GC-MS. Data are deconvoluted using commercial software such as MarkerLynx or publicly available software such as MZmine or XCMS. Data are presented visually for a holistic view of the metabolome with GEDI, or are mined for biomarkers with the machine-learning algorithm Random Forests.

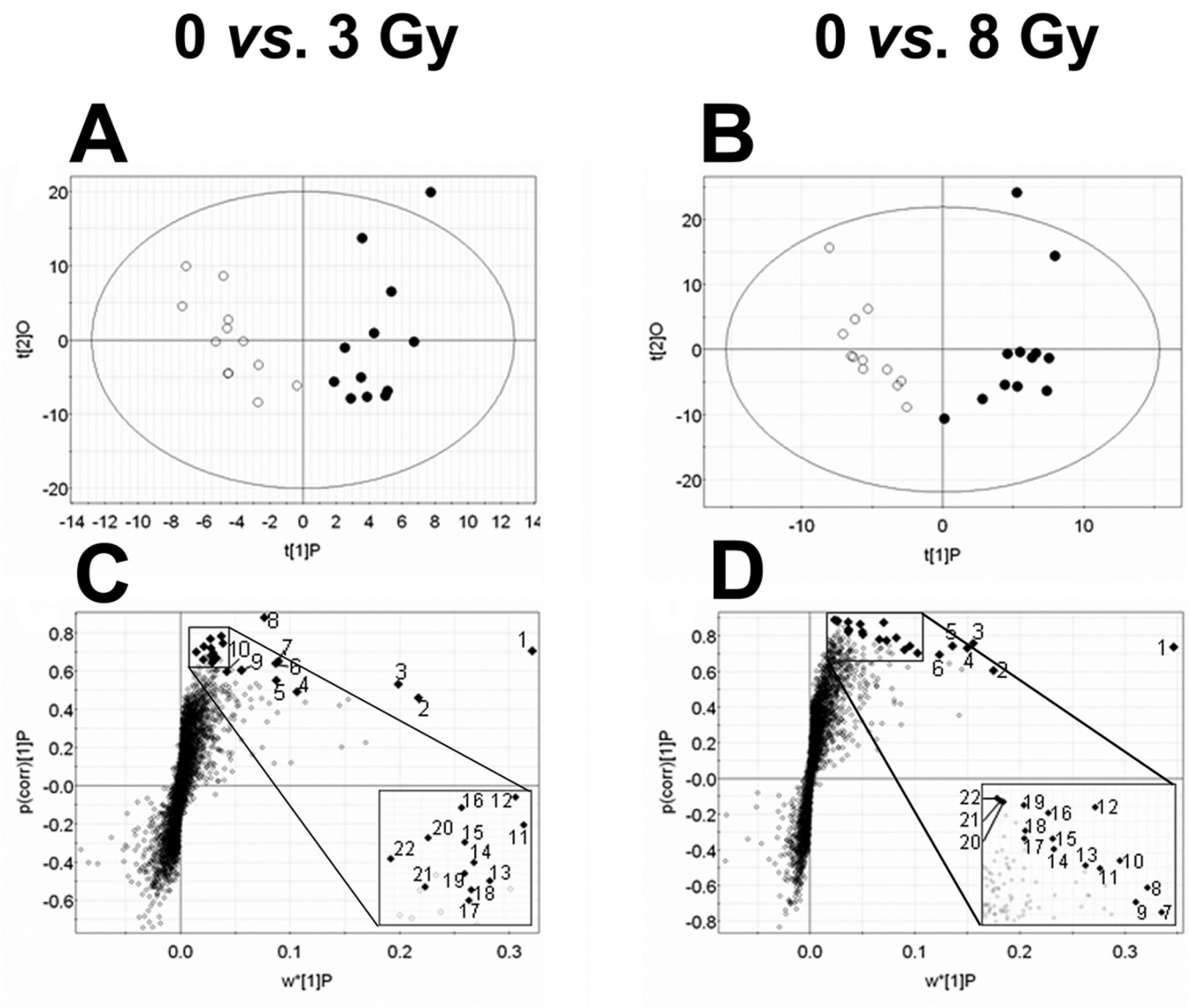

Figure 4.

OPLS scores and loadings plots for urine samples from control and control (○) and irradiated (●) mice for doses of 3 (panel A) and 8 Gy (panel B) show class separation based on exposure status. Ions are found to be elevated in urine from mice exposed to 3 Gy (panel C) and 8 Gy (panel D) compared to the respective controls. Loadings reveal ions in a spatial relationship to the class separation. At each dose, the 22 ions that serve as candidate biomarkers of radiation exposure are indicated. Taken from Tyburski et al. (2008). Reprinted with permission from *Radiation Research*. Copyright (2008).

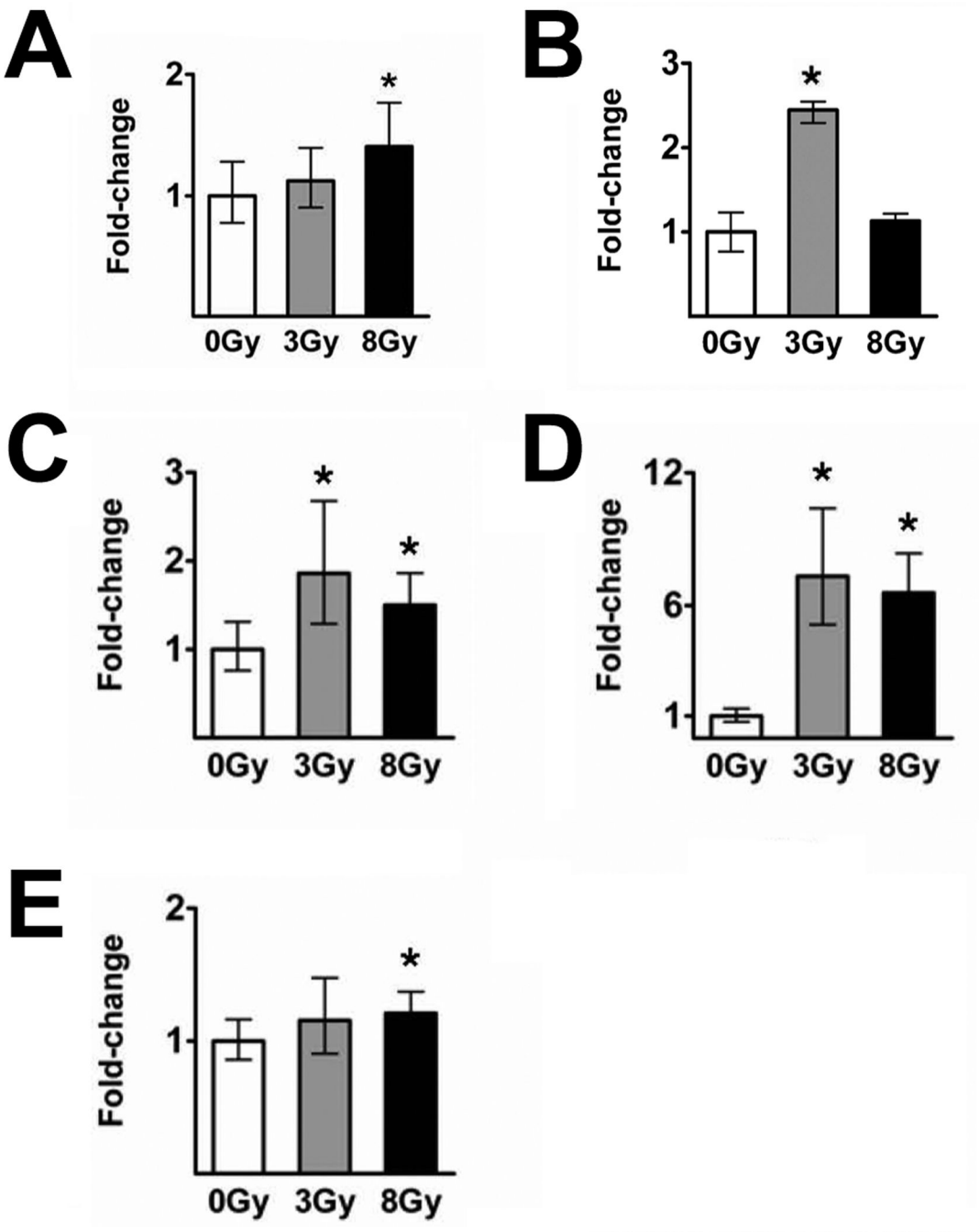

Figure 5.

Relative increases in urinary creatinine and biomarkers at 3 and 8 Gy over those in sham-irradiated animals. Panel A: Creatinine; panel B: 3-hydroxy-2-methylbenzoic acid 3-*O*-sulfate; panel C: *N*-hexanoylglycine; panel D: β-thymidine; panel E: taurine. All data for the quantified biomarkers (panels C–E) were normalized to the creatinine concentration (expressed as μmol/mmol creatinine). Data for 3-hydroxy-2-methylbenzoic acid 3-*O*-sulfate (panel B) are based on relative peak areas and normalized to creatinine. Asterisks indicate statistically significant elevations over controls. Data are means with 95% confidence intervals. Taken from Tyburski et al. (2008). Reprinted with permission from *Radiation Research*. Copyright (2008).

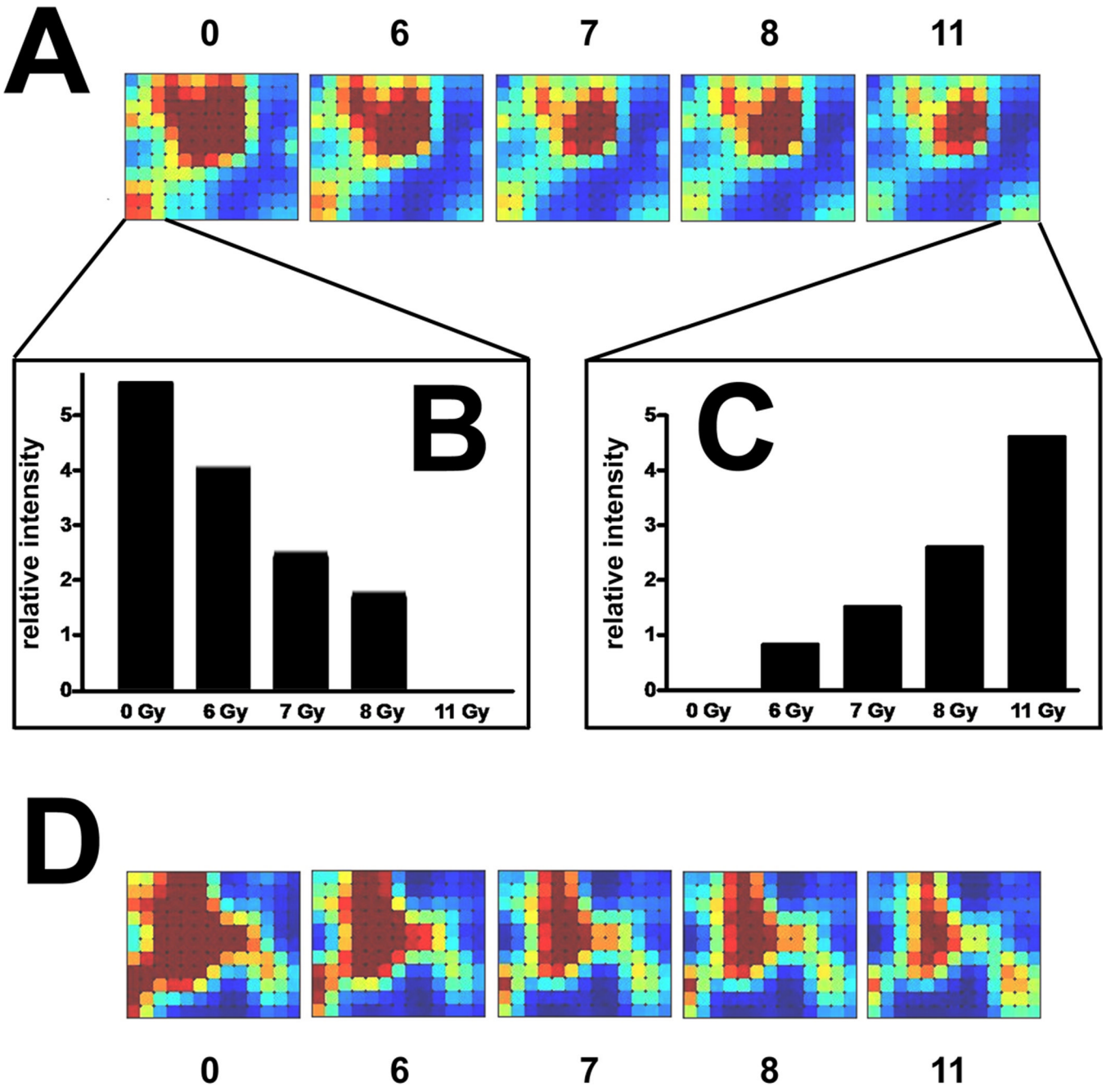

Figure 6.

Dose response of the mouse urinary metabolome to γ radiation. Panel A: Self-organizing maps that give a holistic view of the urinary metabolome in a 13 × 11 matrix (average of 42 ions per cell) constructed with GEDI software. Data used comprise approximately 6,000 ESI- ions. Panel B: Sum total of relative intensities of negative ions in a 3 × 3 matrix in bottom left-hand corner of the maps, with background subtraction (values for 11 Gy). There is a clear decrease in radiation dose response in biomarkers in this region of the metabolome. Panel C: Sum total of relative intensities of negative ions in a 3 × 3 matrix in bottom right-hand corner of the maps, with background subtraction (values for 0 Gy). There is a clear increase in radiation dose response in biomarkers in this region of the metabolome.

Panel D: Self-organizing maps that give a holistic view of the urinary metabolome in a 13 × 11 matrix (average of 42 ions per cell) constructed with GEDI software. Data used comprise approximately 6,000 ESI+ ions. Note that the areas of the positive ion maps that increase and decrease with radiation dose correspond to the areas of the negative-ion maps that increase and decrease with radiation dose (panel A). Taken from Tyburski et al. (2008). Reprinted with permission from *Radiation Research*. Copyright (2008).

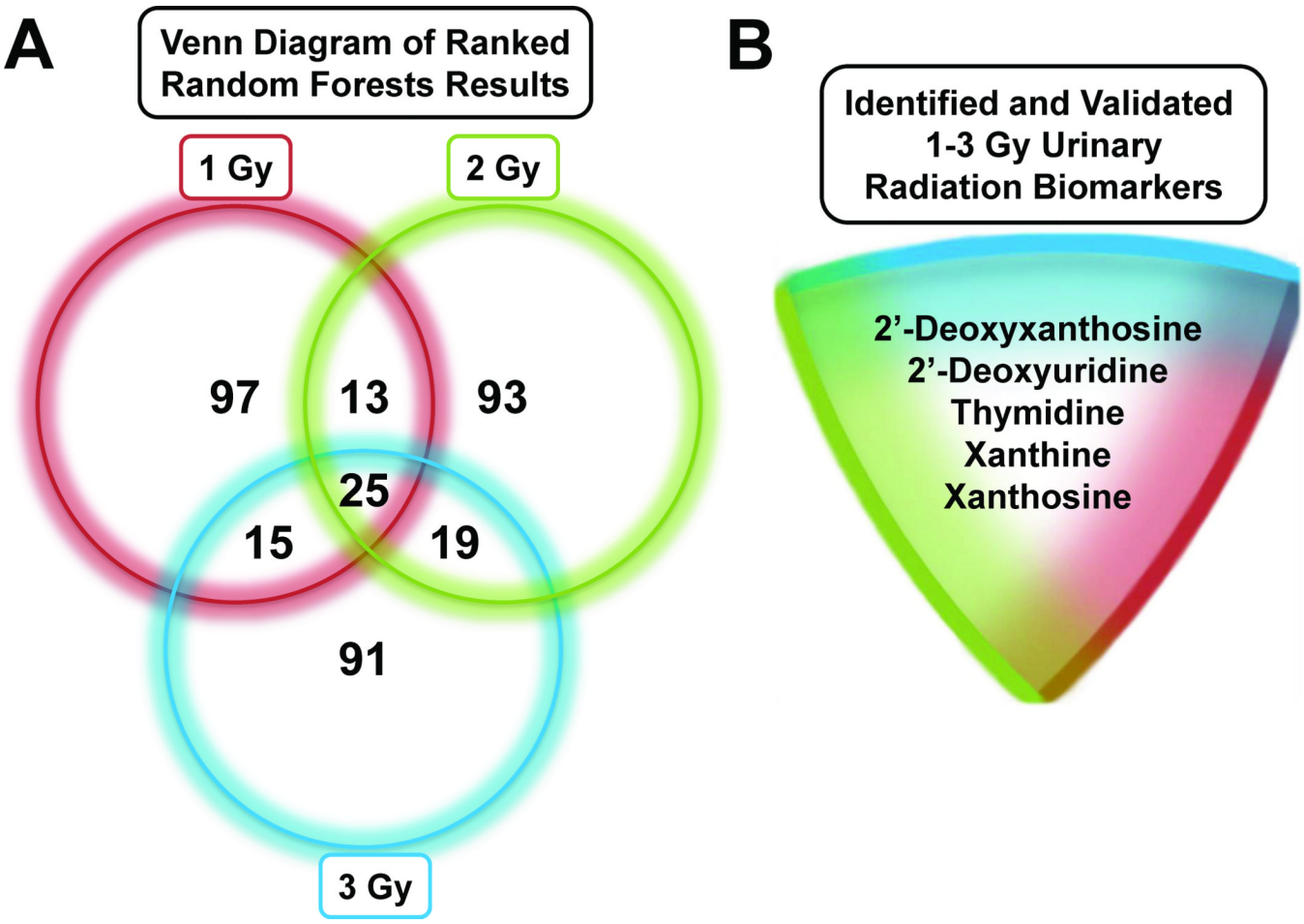

Figure 7.

The top 150 ranked important variables that contribute to the Random Forests classification of 0 vs. 1 Gy, 0 vs. 2 Gy, and 0 vs. 3 Gy were analyzed with a Venn Diagram (A). Common to all three doses were 25 variables, and those that were ultimately identified and validated (B) are 2'-deoxyxanthosine, 2'-deoxyuridine, thymidine, xanthine and xanthosine.

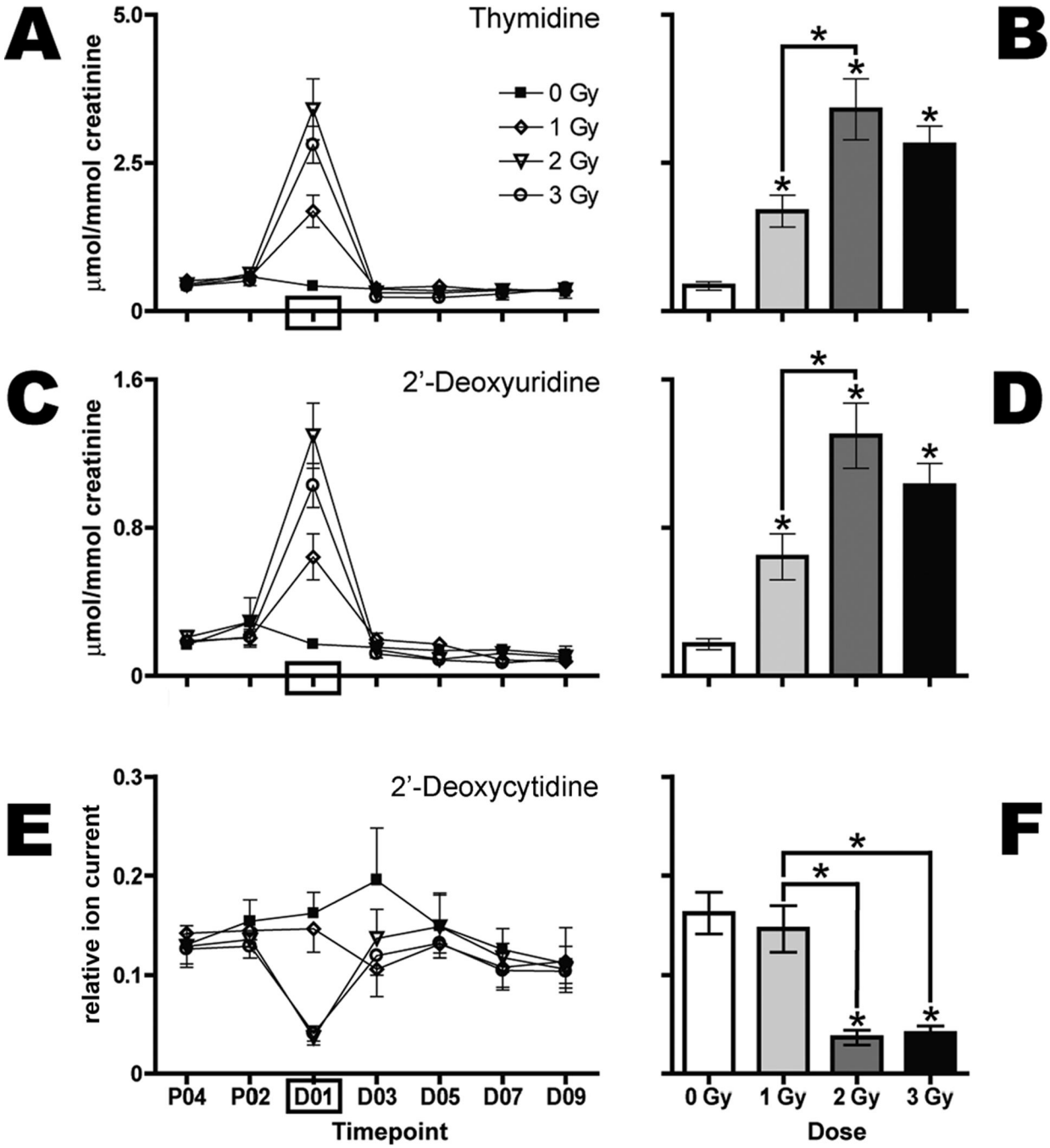

Figure 8.

Gamma-radiation exposure elicits dose-dependent increases in urinary excretion of dT and dU during the first 24 h after exposure and a decrease in urinary excretion of dC. Urine samples were collected prior to (P04, P02) and after (D01, D03, D05, D07, D09) exposure to 0 (■), 1 (◊), 2 (▽), or 3 Gy (○) Gy (n = 6 per dose), and were analyzed by UPLC-TOFMS. Thymidine (panels A and B) and dU (panels C and D), expressed as mean µmol/mmol creatinine and stratified by dose, are shown over time (panels A and C). 2'-Deoxycytidine (panels E and F), expressed as relative ion current (normalized against creatinine), is shown over time (panel E). Mean normalized concentrations of dT (panel B), dU (panel D) and the relative concentration of dC (panel F) in urine from mice exposed to 1,

2, or 3 Gy were compared to the corresponding means of sham controls (0 Gy) at day 1 after exposure (D01) by a two-tailed t-test with unequal variances and $\alpha = 0.05$. Comparisons of mean normalized concentrations of dT, dU, and dC among the three groups of exposed mice were made with one-way ANOVA with Bonferroni correction and $\alpha = 0.05$. Error bars represent ± SEM, and * indicates $P < 0.05$. Taken from Tyburski et al. (2009). Reprinted with permission from *Radiation Research*. Copyright (2009).

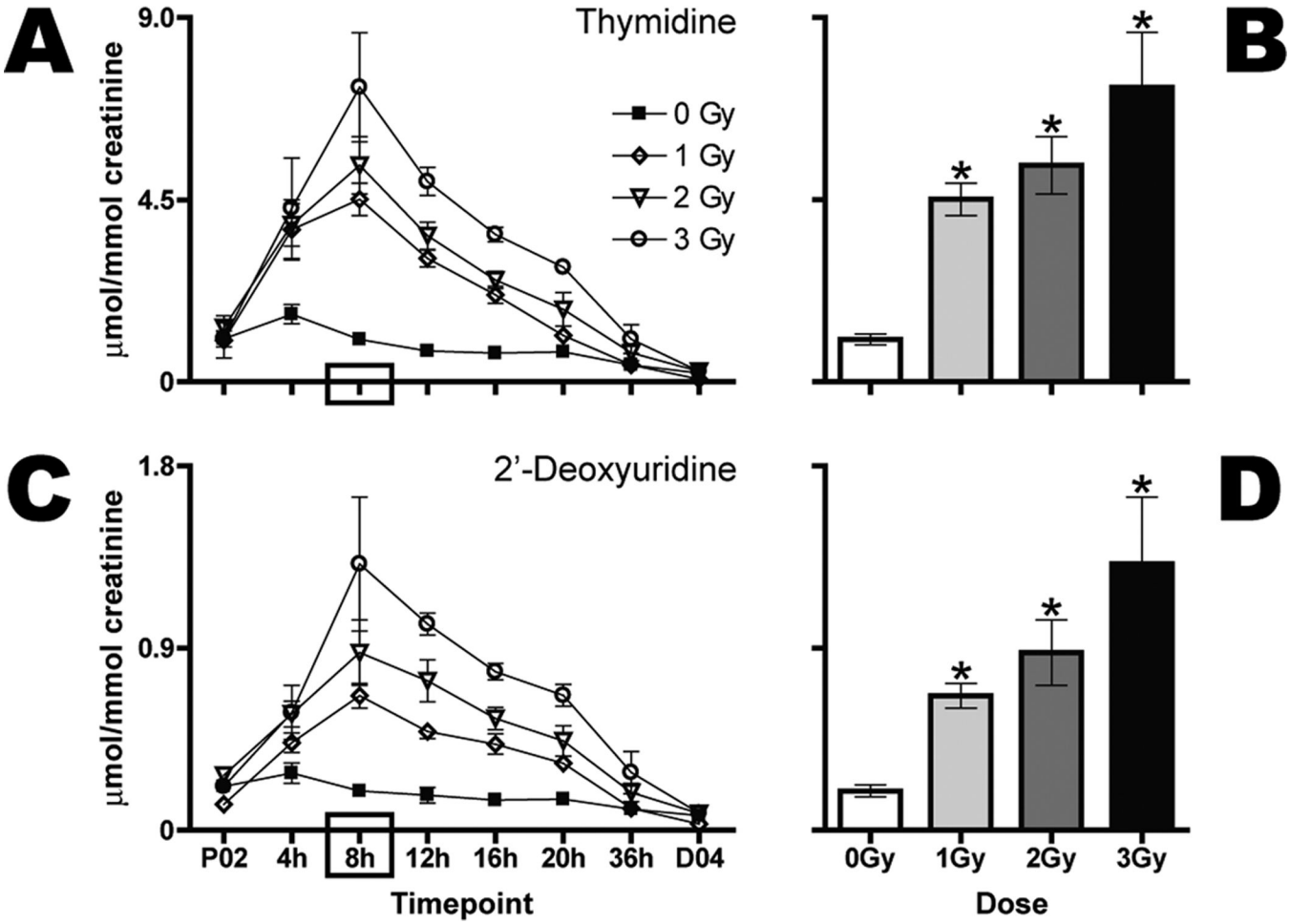

Figure 9.

Gamma-radiation exposure elicits dose-dependent increases in urinary excretion of dT and dU as early as 4 h after exposure. Urine samples were collected prior to (P02) and every 4 h after (4, 8, 12, 16, and 20 h) exposure to 0 (■), 1 (◊), 2 (▽), or 3 (○) Gy (n = 6 per dose) radiation. Urine was collected over 16 h (36 h) and later for a full 24 h at day 4 after exposure (D04). Thymidine (panels A and B) and dU (panels C and D) expressed as mean μmol/mmol creatinine stratified by dose are shown over time (panels A and C). Mean normalized concentrations of dT (panel B) and dU (panel D) for each dose at 8 h were compared to the respective sham control by a two-tailed t-test; unequal variances with $\alpha = 0.05$ were assumed. Comparisons of mean normalized concentrations among the three groups of exposed mice were made with one-way ANOVA with Bonferroni correction and $\alpha = 0.05$. Error bars represent ± SEM, and * indicates $P < 0.05$. Taken from Tyburski et al. (2009). Reprinted with permission from *Radiation Research*. Copyright (2009).

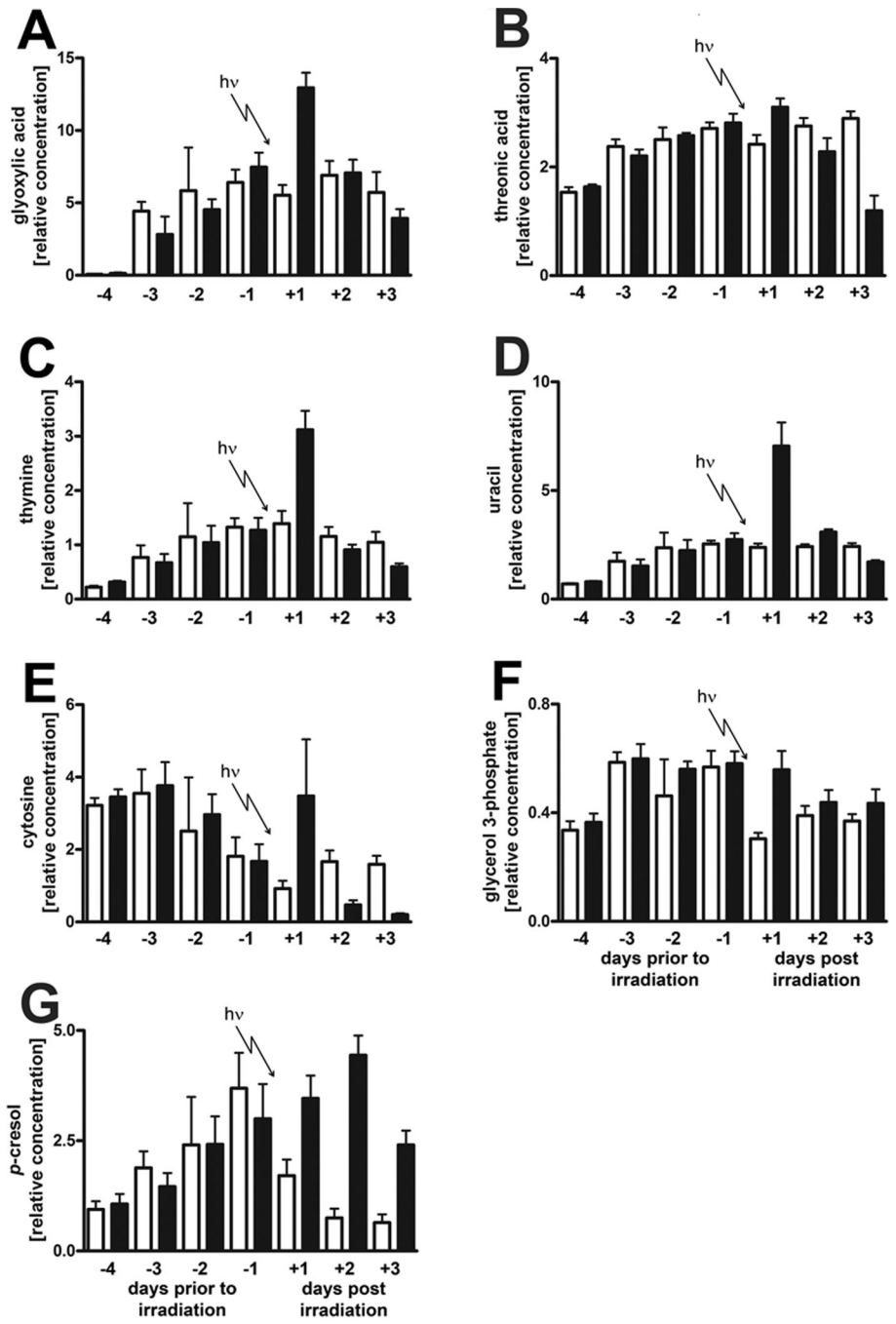

Figure 10.

Trends in glyoxylic acid (panel A), threonic acid (panel B), thymine (panel C), uracil (panel D), cytosine (panel E), glycerol 3-phosphate (panel F), and *p*-cresol (panel G) excretion for 6 sham rats and for 6 rats exposed to 3 Gy γ-radiation after 4 days of acclimation to metabolic cages. Urines were collected on each of day −4, −3, −2, −1, +1, +2, and +3 relative to the radiation dose. For the determination of uracil (panel D), urines were treated with urease to remove the large interfering peak of urea that prevented measurement of uracil. Open bars (□) and filled bars (■) are for sham irradiated and radiated rats, respectively. Error bars represent ± 1 S.D. Taken from Lanz et al. (2009). Reprinted with permission from *Radiation Research*. Copyright (2009).

Table 1

A glossary of commonly used terms in mass spectrometry-based radiation metabolomics.

Term	Definition
Gray	The SI unit of absorbed radiation dose. One Gray is the amount of radiation that deposits 1 Joule of energy per kilogram of matter. 1 Gray (Gy) = 100 rad.
Rad	A commonly used measurement for absorbed dose. 100 rad = 1 Gy.
Rem	A commonly used measurement for equivalent dose. 100 rem = 1 Sv.
Sievert	The SI unit that refers to the amount of any type of radiation that produces roughly the equivalent biological effect as 1 Gy of γ radiation. 1 Sv = 100 rem.
Metabolome	The collection of all metabolites present in a biological fluid, tissue, or organism. The observed metabolome is highly context- and analytical platform-dependent.
Metabolomics	The global qualitative and quantitative profiling of all small molecules present in a biological matrix. Commonly associated with analytical platforms other than NMR. This includes hyphenated techniques such as liquid chromatography-coupled with mass spectrometry.
Metabonomics	Virtually identical to metabolomics, but is more commonly associated with NMR-based profiling of biological matrices.
Projection to Latent Structures Discriminant Analysis (PLS-DA)	Also known as partial least squares. A supervised method that rotates the PCA model to maximize separation of classes.
Orthogonal Projection to Latent Structures (OPLS)	Similar to PLS-DA but concentrates class variation into the first component to thereby simplify interpretation. Any remaining variation unrelated to class membership is explained by subsequent components.
Principal Components Analysis (PCA)	A dimension reduction technique whereby multi-dimensional data sets are reduced to lower dimensions to uncover latent variables. The first component explains the maximum variation in the data; each successive component explains the remaining (or as much as possible) dataset variation.
Random Forests	An ensemble of decision trees based on the classification and regression-tree algorithm. Useful to mine metabolomics data with the variable importance measure (and Gini index).
GEDI	Gene Expression Dynamics Inspector. Based on the self- organizing map algorithm. Useful to present a holistic or systems view of metabolomics data without the need to determine the identification of any metabolites.

Table 2

Comparison of proteomic and metabolomic data from independent experiments in which human fibroblasts were γ-irradiated

PROTEOMICS IN FIBROBLASTS (10 Gy)			METABOLOMICS IN TK6 (1 Gy)	
PROTEIN	UP OR DOWN	REACTION	METABOLITE	UP OR DOWN
Adenylate kinase [2.7.4.3]	↑	AMP→ADP	AMP	↓
Phosphodiesterase [3.1.4.17]	↓	cAMP→AMP cGMP→GMP	AMP GMP	↓ ↓
Phosphoribosylformylglycinamidine synthase [6.3.5.3]	↓	ATP→ADP	AMP	↓
HPGRT [2.4.2.8]	↓	adenine→AMP guanine→GMP	AMP GMP	↓ ↓
Ribonucleoside-diphosphate reductase [1.17.4.1]	↑	ADP→dADP GDP→dGDP CDP→dCDP UDP→dUDP	AMP GMP UMP	↓ ↓ ↓
Pyruvate kinase [2.7.1.40]	↑	pyruvate→phosphoenolpyruvate ATP→ADP GTP→GDP	 AMP GMP	 ↓ ↓
Inosine 5’-monophosphate dehydrogenase [1.1.1.205]	↓	AMP→IMP→XMP→GMP	AMP	↓
Guanine deaminase [3.5.4.3]	↓	guanine→xanthine	GMP	↓